A Critical Analysis of the Mechanistic Basis of Enantioselectivity in the Bis-Cinchona Alkaloid Catalyzed Dihydroxylation of Olefins

E. J. Corey* and Mark C. Noe

Contribution from the Department of Chemistry, Harvard University, Cambridge, Massachusetts 02138

Received April 15, 1996[⊗]

Abstract: This paper presents a critical analysis of two transition state models for the bis-cinchona alkaloid catalyzed enantioselective dihydroxylation of olefins using a broad range of experimental data. In one model (Sharpless) the transition state resembles a metallaoxetane structure formed by [2 + 2] cycloaddition of Os═O and C═C, and in the other the transition state is a five-membered structure in which one axial and one equatorial oxygen of cinchona bound OsO_4 are becoming attached to the olefinic carbons by a [3 + 2] cycloaddition process from an Os−olefin π-complex (CCN model, Figure 1). Data on the enantioselectivity of the asymmetric dihydroxylation of a wide variety of olefinic substrates and on the selectivity of a range of catalyst structures agree well with expectations based on the CCN model, but not the Sharpless model.

Introduction

The conversion of olefins to 1,2-diols by dihydroxylation using the reagent osmium tetraoxide has long been a valuable reaction for organic synthesis.[1] In recent years this transformation has been upgraded to an enantioselective method through the use of chiral 1,2-diamines with stoichiometric OsO_4[2] or chiral cinchona alkaloid derivatives with catalytic quantities of OsO_4 and a stoichiometric co-oxidant.[3] The cinchona-catalyzed (Sharpless) version of the enantioselective dihydroxylation reaction is especially practical because it requires much less of the expensive OsO_4. Both the chiral 1,2-diamine and the cinchona alkaloid mediated processes are capable of high enantioselectivity, and both types of ligand strongly accelerate the rate of reaction of OsO_4 with olefins. Until recently very little was known regarding the fundamental basis for enantioselectivity and ligand acceleration. Moreover, two different types of mechanisms have been advanced for the amine-accelerated dihydroxylation of olefins by OsO_4: (1) a [3 + 2] cycloaddition (Criegee) pathway leading to the cyclic Os(VI) ester intermediate and (2) a [2 + 2] cycloaddition of olefin and OsO_4 either preceded or followed by coordination with catalytic amine (Sharpless pathway). We believe that the evidence available at this time strongly favors the [3 + 2] mechanistic path. The main purpose of this paper is to provide a critical comparison of the [3 + 2] and [2 + 2] mechanistic alternatives. This analysis is especially appropriate now, since many chemists are attracted to the [2 + 2] mechanism because of the analogy with the well-known and facile [2 + 2] cycloadditions which are involved in olefin metathesis. Moreover, in the most recent review[3] on enantioselective dihydroxylation of olefins, there was little discussion of the [3 + 2] pathway. Recent studies in this laboratory have provided strong evidence that the chiral 1,2-diamine-accelerated enantioselective dihydroxylation of olefins by OsO_4 occurs via a pathway which is bidentate with respect to the diamine and unlikely to involve a [2 + 2] intermediate.[4]

The development of the Sharpless asymmetric dihydroxylation of olefins using various cinchona alkaloid derivatives as chiral monodentate amine ligands for OsO_4 was accomplished by the synthesis and testing of many compounds. Starting from the initial observation that dihydroquinidine acetate promotes modestly enantioselective dihydroxylation of simple olefins such as (*E*)-stilbene or styrene,[5] Sharpless and co-workers screened many cinchona alkaloid derivatives with gradual improvement of enantioselectivity.[3] The most efficient ligands for promoting face-selective dihydroxylation of olefins such as styrene (96% ee) were found to be bis-cinchona alkaloids such as the $(DHQD)_2PHAL$ system which is shown. In our research the most heavily studied system has been that based on the pyridazine-linked ligand **1**, $(DHQD)_2PYDZ$, since this readily available bis-cinchona alkaloid derivative was found to be more amenable to X-ray crystallographic studies. ^1H NMR studies showed that, although **1** is conformationally flexible in solution,

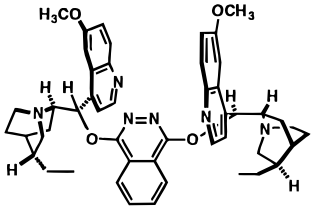

$(DHQD)_2PHAL$
(Sharpless)[6]

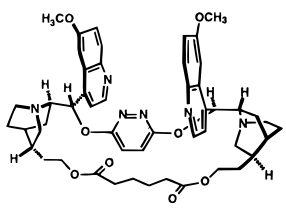

Adipate-bridged $(DHQD)_2PYDZ$[7a]

[⊗] Abstract published in *Advance ACS Abstracts,* October 15, 1996.

(1) For background and review, see: Schröder, M. *Chem. Rev.* **1980**, *80*, 187.

(2) (a) Yamada, T.; Narasaka, K. *Chem. Lett.* **1986**, 131. (b) Tokles, M.; Snyder, J. K. *Tetrahedron Lett.* **1986**, *27*, 3951. (c) Tomioka, K.; Nakajima, M.; Koga, K. *J. Am. Chem. Soc.* **1987**, *109*, 6213. (d) Hirama, M.; Oishi, T.; Itô, S. *J. Chem. Soc., Chem. Commun.* **1989**, 665. (e) Corey, E. J.; Jardine, P. D.; Virgil, S.; Yuen, P.-W.; Connell, R. D. *J. Am. Chem. Soc.* **1989**, *111*, 9243. (f) Tomioka, K.; Nakajima, M.; Koga, K. *Tetrahedron Lett.* **1990**, *31*, 1741. (g) Hanessian, S.; Meffre, P.; Girard, M.; Beaudoin, S.; Sancéau, J.-Y.; Bennani, Y. *J. Org. Chem.* **1993**, *58*, 1991.

(3) For a review of the catalytic asymmetric dihydroxylation of olefins, see: Kolb, H. C.; VanNieuwenhze, M. S.; Sharpless, K. B. *Chem. Rev.* **1994,** *94*, 2483.

(4) Corey, E. J.; Sarshar, S.; Azimioara, M. D.; Newbold, R. C. Noe, M. C. *J. Am. Chem. Soc.*, in press.

(5) Hentges, S. G.; Sharpless, K. B. *J. Am. Chem. Soc.* **1980**, *102*, 4263.

(6) Sharpless, K. B.; Amberg, W.; Bennani, Y. L.; Crispino, G. A.; Hartung, J.; Jeong, K.-S.; Kwong, H.-L.; Morikawa, K.; Wang, Z.-M.; Xu, D.; Zhang, X.-L. *J. Org. Chem.* **1992**, *57*, 2768.

S0002-7863(96)01233-4 CCC: $12.00

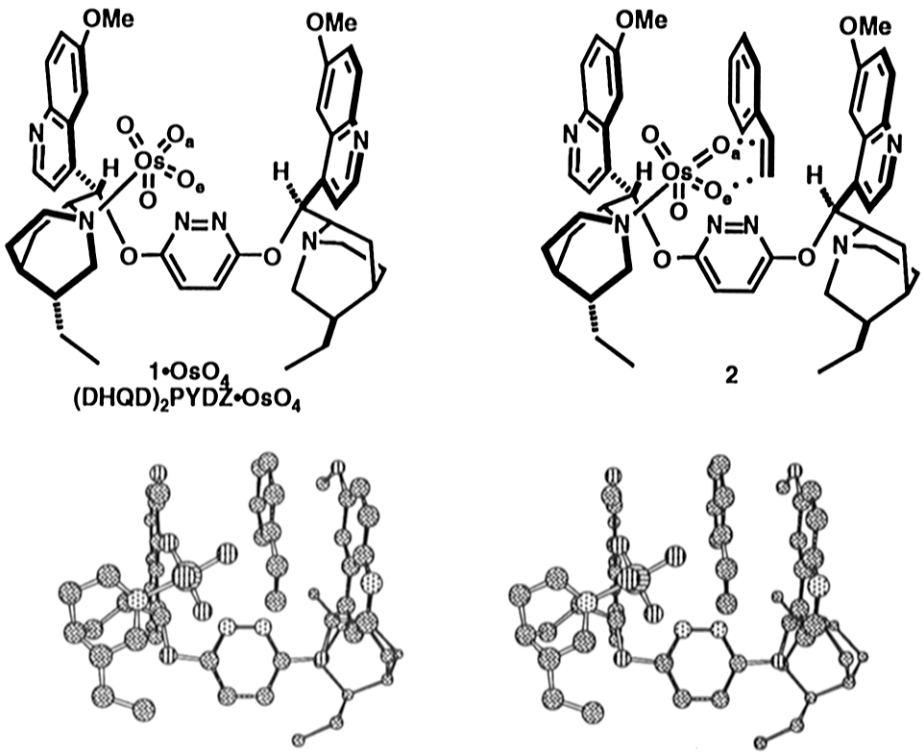

Figure 1. Stereopair representation of the complex of olefin, OsO_4, and **1** that leads to the observed enantiomer of styrene glycol *via* the [3 + 2] cycloaddition pathway. The hydrogen atoms in this and subsequent figures are omitted for clarity.

coordination of the two quinuclidine nitrogens, e.g. to OsO_4 or CH_3^+ (as the bis-methiodide salt), rigidified the structure to the favored conformation which is shown.[7a,b] The same structure was revealed in X-ray crystallographic studies of the bis-methiodide of **1** or of the adipate-bridged analog of **1** which is shown.[7a,b] The rates of dihydroxylation and the enantioselectivities observed with **1** and the adipate-bridged analog were essentially the same for a series of different olefins.[7a] These and a variety of other studies on the mechanistic basis for enantioselectivity in the Sharpless asymmetric dihydroxylation[7] led to the proposal of the transition state arrangement **2** shown in Figure 1 for the enantioselective dihydroxylation of styrene, involving [3 + 2] cycloaddition of osmium tetraoxide to the double bond, and designated herein as the CCN (for Criegee−Corey−Noe) model. The transition states for the dihydroxylation of 1-alkenes such as 1-decene were proposed to be analogous to that shown in Figure 1. With the 2,3-bond *s-cis*, the *n*-alkyl is in van der Waals contact between the two methoxyquinoline units. Terminal olefins with bulky substituents such as *tert*-butyl are dihydroxylated with low enantioselectivity; such groups are too large for the binding pocket. The critical interactions between the catalyst and the substrate which favor transition state **2** for enantioselective dihydroxylation have been described previously and are restated below.[7] This model provides the simplest and clearest explanation for the high enantioselectivities observed in the asymmetric dihydroxylation of a wide variety of substrates. Moreover, the CCN model has demonstrated considerable heuristic value in the development of several novel applications of and catalysts for the dihydroxylation reaction.[8]

Despite these attractive features, the [3 + 2] cycloaddition mechanism for enantioselective dihydroxylation does not seem to have been universally accepted. One complication arises from the fact that different versions of the [2 + 2] pathway have been proposed,[3,9] and it is not clear whether the ligand coordinates to osmium before or after [2 + 2] cycloaddition. Rate enhancement by the catalytic amine is unexplained. These ambiguities, coupled with the simplicity of the substrates that have been used to argue for the validity of this model based upon metallaoxetane stability, complicate the case for or against the Sharpless model. Unfortunately, no analysis has been made of its applicability to more highly substituted olefins. Sharpless and co-workers attempted to compare the [3 + 2] and [2 + 2] cycloaddition models only for the dihydroxylation of various substituted styrenes.[9c] The main point in this discussion was that the enantioselectivity observed for the dihydroxylation of 3-*tert*-butylstyrene (95%) is very close to that for styrene (97%) and that these results "are consistent only with our model".[9c] That statement is not credible. Reference to Figure 1 will confirm that a *tert*-butyl substituent can be placed at the forward *meta* position of styrene in the CCN model shown in Figure 1 without appreciable destabilization or steric repulsion. In a recent review (ref 3, p 2488), this result with 3-*tert*-butylstyrene was also claimed to be "inconsistent" with the CCN model.

(7) (a) Corey, E. J.; Noe, M. C. *J. Am. Chem. Soc.* **1993**, *115*, 12579. (b) Corey, E. J.; Noe, M. C.; Sarshar, S. *Tetrahedron Lett.* **1994**, *35*, 2861. (c) Corey, E. J.; Noe, M. C.; Grogan, M. J. *Tetrahedron Lett.* **1994**, *35*, 6427. (d) Corey, E. J.; Noe, M. C. *J. Am. Chem. Soc.* **1996**, *118*, 319. (e) Corey, E. J.; Noe, M. C.; Sarshar, S. *J. Am. Chem. Soc.* **1993**, *115*, 3828.

(8) For the development of the asymmetric dihydroxylation of allylic 4-methoxybenzoates and derivatives, see: (a) Corey, E. J.; Guzman-Perez, A.; Noe, M. C. *J. Am. Chem. Soc.* **1995**, *117*, 10805. (b) Corey, E. J.; Guzman-Perez, A.; Noe, M. C. *Tetrahedron Lett.* **1995**, *36*, 3481. (c) Corey, E. J.; Noe, M. C.; Ting, A. *Tetrahedron Lett.*, in press. For the development of the enantioselective terminal dihydroxylation of oligoterpenes, see: (d) Corey, E. J.; Noe, M. C.; Lin, S. *Tetrahedron Lett.* **1995**, *36*, 8741. For the development of the kinetic resolution of racemic allylic esters, see: (e) Corey, E. J.; Noe, M. C.; Guzman-Perez, A. *J. Am. Chem. Soc.* **1995**, *117*, 10817.

(9) (a) Norrby, P.-O.; Kolb, H. C.; Sharpless, K. B. *Organometallics* **1994**, *13*, 344. (b) Norrby, P.-O.; Kolb, H. C.; Sharpless, K. B. *J. Am. Chem. Soc.* **1994**, *116*, 8470. (c) Becker, H.; Ho, P. T.; Kolb, H. C.; Loren, S.; Norrby, P.-O.; Sharpless, K. B. *Tetrahedron Lett* **1994**, *35*, 7315. (d) Norrby, P.-O.; Becker, H.; Sharpless, K. B. *J. Am. Chem. Soc.* **1996**, *118*, 35. (e) Sharpless, K. B.; Teranishi, A. Y.; Bäckvall, J. E. *J. Am. Chem. Soc.* **1977**, *99*, 3120. (f) Jørgensen, K. A.; Schiøtt, B. *Chem. Rev.* **1990**, *90*, 1483.

Scheme 1. Proposed CCN Pathway for the Production of the Osmium(VI) Ester of Styrene from Styrene and **1**·OsO_4.

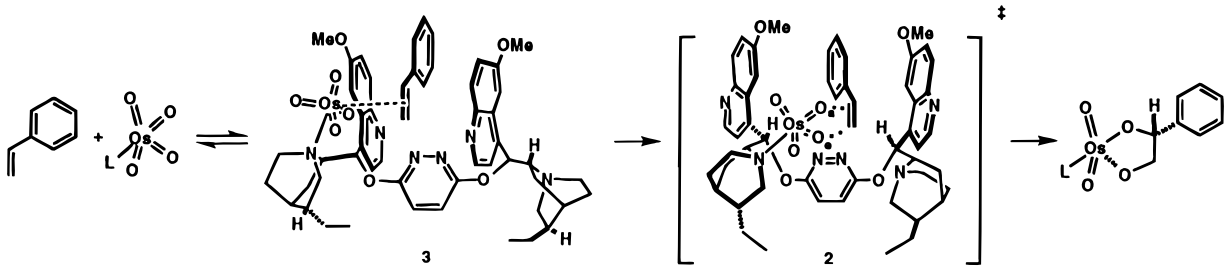

In order to clarify the relative merit of the [3 + 2] and [2 + 2] cycloaddition models, we shall begin with the analysis of a number of important test substrates which react with high enantioselectivity in the asymmetric dihydroxylation and compare expectations based on the two mechanisms with the experimental data. It will be shown that in each of these critical cases the [3 + 2] cycloaddition model provides a simple and clear explanation for the high levels of face selectivity in the asymmetric dihydroxylation and that the Sharpless metallaoxetane model is inconsistent with the experimental results.

Description of the Mechanistic Models. The CCN [3 + 2] cycloaddition pathway for the enantioselective dihydroxylation is shown for the case of styrene in Figure 1. The ligand geometry in Figure 1 corresponds *exactly* to that indicated by X-ray and ^{1}H NMR (including NOE) studies of the bis-methiodide;[7b] this specific geometry forms the basis for all of the CCN pathways and figures presented herein.[7a,b] The mono-methiodides (and other mono quaternary ammonium salts) of ligands such as **1** are generally somewhat more effective or equivalent to the bis-amines and lead to conformationally more rigid structures.[7b] It seems likely that mono OsO_4 complex **1** is similarly rigidified in *t*-BuOH−H_2O (the most effective medium for enantioselectivity in the catalytic dihydroxylation reaction) by hydrogen bonding of solvent to the standby quinuclidine nitrogen. The spacing between the parallel methoxyquinoline rings in Figure 1 is indicated to be 7.2 Å from X-ray data. The HCCH dihedral angle for the quinuclidine−benzylic carbon bond is indicated to be fixed near 90° both from ^{1}H NMR coupling constant and X-ray data.[7b] The C−O−C(pyridazine) unit is coplanar with the pyridazine ring with a large barrier to rotation (from X-ray and variable temperature ^{1}H NMR studies up to 150 °C). Other rotational motions of **1**·OsO_4 from the geometry shown are possible about the bonds from the quinoline ring and the pyridazinyloxy group to the benzylic carbon, but these are likely to be modest because of nonbonded steric repulsions which set in with deviations from the geometry shown in Figure 1.

The CCN pathway has the following characteristics: (1) a preference for the U-shaped conformation of the catalyst **1**·OsO_4, which has the ability to bind olefinic substrates in a binding pocket composed of the two parallel methoxyquinoline units, *N*-coordinated OsO_4 and the pyridazine spacer,[7a,b] (2) initial complexation between the double bond of the substrate and the Os center of quinuclidine-bound OsO_4 which adds an additional binding contact between the catalyst and the substrate,[7d] (3) the proximity of one axial oxygen (O_a) and one equatorial oxygen (O_e) to the olefinic carbons of the bound substrate,[7a,b] and (4) a minimum motion pathway from this arrangement *via* a [3 + 2] cycloaddition reaction that directly produces the pentacoordinate osmium(VI) ester in the energetically most favorable geometry.[7a,b] The acceleration of face-selective dihydroxylation by the bis-cinchona alkaloid derivative **1** is derived from three factors: (1) shortening (i.e. strengthening)[4] of the quinuclidine N−Os bond during reaction, (2) rotation of the N−Os bond from the eclipsed to the more favorable staggered geometry in going from the initial bound complex to the transition state for dihydroxylation,[7] and (3) van der Waals binding of the catalyst and the substrate to reduce the entropic cost of the reaction. Dihydroxylation of the opposite olefin face is less favorable because there is no three-dimensional arrangement for effective binding of the substrate with *N*-coordinated OsO_4 and the U-shaped catalyst binding pocket.[7]

The observation of Michaelis−Menten kinetic behavior,[7d] which implies the intermediacy of a reversibly and rapidly formed olefin−catalyst complex **3** (Scheme 1), is fully consistent with the [3 + 2] cycloaddition mechanism. Complex **3** involves not only a donor−acceptor (d-π) interaction between the double bond and osmium but also attractive van der Waals interactions between the substrate and the enzyme-like U-shaped binding pocket, as shown. This pathway accords with all available experimental data on the bis-cinchona/OsO_4-catalyzed enantioselective dihydroxylation of olefins, including the observation[10] of modest nonlinearity (temperature breaks) in Eyring-type diagrams. As has been pointed out in an extensive discussion of the application of Eyring diagrams to chemical selectivity, nonlinear Eyring plots "should be observable" for systems with Michaelis−Menten kinetics.[11]

At least two variants on the [2 + 2] cycloaddition pathway have been advanced by Sharpless,[3,5,9d,e] and these are summarized in Scheme 2. The early Sharpless proposal[5] emphasized the importance of ligand-based stabilization of the metallaoxetane intermediate, formed by [2 + 2] cycloaddition of the substrate olefin with ligand-bound OsO_4, without specifying a rate-limiting step. Rearrangement of the putative osmaoxetane leading to the observed [3 + 2] cycloadduct was assumed. This model was later revised apparently on the basis of a lack of precedence for the cycloaddition of the olefin to the 18-electron L·OsO_4 species.[9d] This revised pathway for production of the diol *via* the [2 + 2] cycloadduct, which corresponds to path B of Scheme 2, was based on the assumption of rapid reversible formation of the metallaoxetane from olefin and OsO_4 and subsequent coordination of the ligand which accelerates rearrangement to the osmium(VI) ester.[12] It was proposed that

(10) See: Göbel, T.; Sharpless, K. B. *Angew. Chem., Int. Ed. Engl.* **1993**, *32*, 1329. These authors have argued that nonlinear Eyring plots of enantioselectivity as a function of the reciprocal of temperature for a number of asymmetric dihydroxylation reactions supports a two-step [2 + 2] mechanism, but not a [3 + 2] pathway for these reactions on the assumption that the latter would be a single-step reaction.

(11) (a) Buschmann, H.; Scharf, H.-D., Esser, P. *Angew. Chem., Int. Ed. Engl.* **1991**, *30*, 477. (b) The observation of breaks in enantioselectivity−temperature Eyring plots is readily understood in terms of the intermediacy of the Michaelis−Menten complex **3** and reaction via a [3 + 2] transition state, **2**. Major and minor dihydroxylation pathways, leading to major and minor enantiomeric diols via diastereomeric transition states, each have a pre-equilibrium step and a transition state forming step (i.e. two selectivity steps) with quite different activation enthalpy-entropy balances.[11a] (c) A recent report, which appeared after the preparation of this manuscript, argues in favor of the [2 + 2] pathway over the [3 + 2] mechanism, but does not consider the demonstration[7d] of Michaelis−Menten kinetics. See: Norrby, P.-O.; Gable, K. P. *J. Chem. Soc., Perkin Trans. 2*, **1996**, 171.

Scheme 2. Two of the Sharpless [2 + 2] Cycloaddition Pathways for the Production of the Osmium(VI) Ester of Styrene from Styrene and **1**·OsO_4.

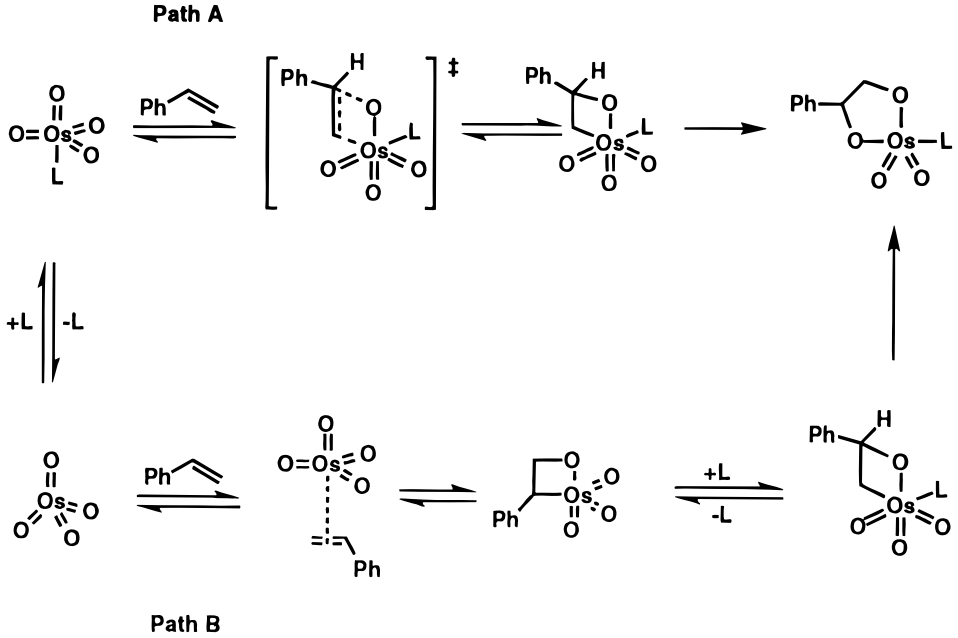

enantioselectivity depends both on the relative stabilities of the diastereomeric [2 + 2] cycloadducts and on the rates at which they rearrange.

The observation of Michaelis−Menten kinetic behavior in the catalytic asymmetric dihydroxylation[7d] indicates that if a metallaoxetane intermediate is formed, its formation must occur rapidly and reversibly, and that the subsequent rearrangement to the [3 + 2] cycloadduct must be rate determining. The Curtin−Hammett principle dictates that for this situation the relative stabilities of the diastereomeric metallaoxetanes are irrelevant to enantioselectivity and that enantioselectivity will depend on the two transition state energies. If the transition state for this rearrangement occurs early, as might be expected from the exothermicity of the Os(VI) ester formation (Hammond principle), then its geometry could resemble that of the intermediate metallaoxetane. In the event of a late transition state which resembles the [3 + 2] transition state, the role of the [2 + 2] adduct is inconsequential and hence superfluous to mechanistic analysis. Because of these considerations and the fact that Sharpless' latest proposal implies that the transition state for rearrangement resembles the metallaoxetane intermediate,[9] the analysis presented in this paper of the [2 + 2] pathway will focus on the stabilities of the diastereomeric metallaoxetanes as determinants of the relative rates of formation of enantiomeric diols. In the most recent arguments presented by Sharpless in favor of the [2 + 2] pathway, a series of *ab initio* calculations of the stabilities of diastereomeric metallaoxetane species derived from Me_3N·RuO_4 and simple olefins was presented. The calculated energies of these intermediates (which use an assumed basis set and neglect electron correlation and relativistic effects) were then assumed to hold for the cinchona alkaloid−OsO_4-catalyzed asymmetric dihydroxylation. In order to compensate for the neglected influence of the cinchona alkaloid ligand on metallaoxetane stability in these calculations, a qualitative molecular mechanics model was formulated based on the *ab initio* work with RuO_4.[9b] The relevance of such approximate calculations based on RuO_4 to the asymmetric dihydroxylation with OsO_4 is unclear. To be of value such calculations would have to be very precise (e.g. ±0.5 kcal/mol). Furthermore, all of these calculations were carried out only for simple substrates, and no analysis of the many approximations was presented. Recent and more rigorous calculations on the reaction of ethylene with OsO_4·NH_3 clearly disfavor the [2 + 2] mechanism.[13] In contrast, for these same substrates, the CCN [3 + 2] cycloaddition model provides a simple and clear understanding of enantioselectivity.

The differential stabilization of the diastereomeric metallaoxetanes in the Sharpless proposal is thought to occur through stabilizing (van der Waals) interactions between one of the substrate substituents and an L-shaped domain composed of a phthalazine linker group and one methoxyquinoline ring of the catalyst.[3] A metallaoxetane intermediate for the enantioselective dihydroxylation of styrene, analogous to that advanced by Sharpless,[3] is shown in Figure 2 for the pyridazine-linked bis-dihydroquinidine system. We had previously shown that the pyridazine- and phthalazine-linked bis-cinchona systems exhibit nearly identical behavior for a range of substrates.[7e] As indicated in Figure 2, the phenyl group of the substrate overlaps with only half of the pyridazine linker group of **1**, with the remainder projecting out toward solvent. There are minimal additional interactions with the substrate and the methoxyquinoline ring that composes one wall of the proposed L-shaped pocket. These observations would suggest that the pyridazine-linked catalyst should be considerably less effective than the phthalazine analog with regard to enantioselectivity, contrary to experimental results.[7e] Furthermore, the minimal contact of the substrate with the forward methoxyquinoline ring (right side) of the catalyst suggests that its replacement with a methoxy group should not affect enantioselectivity. These expectations are inconsistent with the experimental observations (*vide infra*).[7e]

The differential mechanistic analysis of the CCN [3 + 2] and Sharpless [2 + 2] pathways which is the major purpose of

(12) An Os(VI) ester coordinated to a mono-cinchona alkaloid ligand has been characterized by X-ray crystallography. See: Pearlstein, R. M.; Blackburn, B. K.; Davis, W. M.; Sharpless, K. B. *Angew. Chem., Int. Ed. Engl.* **1990**, *29*, 639.

(13) Recent calculations for the reaction of OsO_4·NH_3 with CH_2=CH_2 (GAUSSIAN 94 program at the B3LYP level of density functional theory with the LANLZDZ effective core potential) have indicated that the reaction cannot involve a [2 + 2] intermediate but can proceed via a [3 + 2] pathway with a very low barrier. Dapprich, S.; Vjaque, G.; Maseras, F.; Lledós, A.; Morokuma, K. *J. Am. Chem. Soc.*, submitted. We thank the authors for a preprint of this paper.

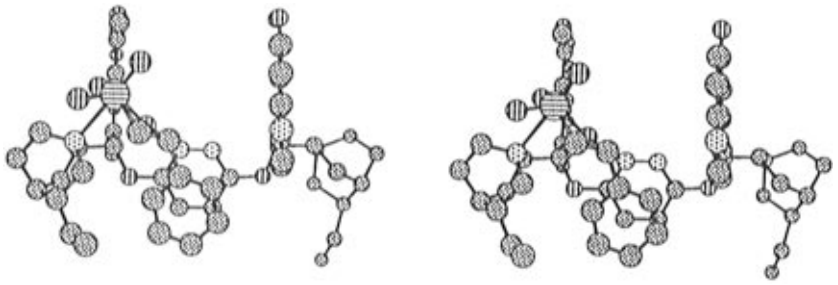

Figure 2. Stereopair representation of the metallaoxetane intermediate derived from styrene, OsO_4, and **1** that leads to the observed enantiomer of styrene glycol.

this paper will be carried out by comparing the approximate three-dimensional representations of the transition states. Three types of comparisons will be made: (1) based on substrate structure for a variety of crucial structural classes, (2) based on changes in the structure of the catalytic ligand, and (3) based on kinetic resolution studies (i.e. relative rates of dihydroxylation) of chiral olefins. A critical aspect of each comparison is the analysis of the interactions between the substrate and the binding regions of the ligand.

The binding regions that provide stabilization for the alternative transition states for the asymmetric dihydroxylation possess very different topological features and dimensions. The U-shaped binding pocket proposed for the CCN [3 + 2] pathway[7] is approximately 6.9 Å wide (measured as the interplanar distance of the two methoxyquinoline walls) and 9−10 Å long (measured from the outer edges of the two methoxyquinoline walls). The L-shaped binding domain proposed by Sharpless for the metallaoxetane intermediate is approximately 5.5 Å wide (measured from the innermost equatorial oxygen of OsO_4 to the plane of the forward methoxyquinoline wall) and has variable length at the bottom of the L depending on the heteroaromatic linker group (3.4 Å long for the pyridazine and 5.7 Å long for the phthalazine linker). A stereoview of the binding region involved in the [2 + 2] dihydroxylation of styrene with the pyridazine linker is shown in Figure 2. In the subsequent discussion of the [2 + 2] mechanism for various substrates we have used the ligand geometry proposed by the Sharpless group for the bis-cinchona−OsO_4 complex in a recent review[3] in which it is stated that "Recent ligand structure−activity studies have shed light on the origin of the enantioselectivity in the AD reaction and demonstrated the importance of an enzyme-like binding pocket present in the "dimeric" cinchona alkaloid ligands, e.g., the phthalazine ligands (Figure 3)." The illustration in their Figure 3 used styrene as the olefinic substrate. The large topological differences between [3 + 2] and [2 + 2] ligand binding suggests that the enantioselectivity of the dihydroxylation of judiciously chosen substrates can serve to distinguish between the pathways. For such a decisive comparison, it is necessary to consider only substrates that are dihydroxylated with high enantioselectivity, and the discussion which follows deals only with such cases. In our judgment, the analysis presented herein overwhelmingly supports the CCN [3 + 2] cycloaddition model but not the metallaoxetane mechanism.

Results and Discussion

Substrate Structure and Enantioselectivity. One important feature of the CCN [3 + 2] mechanistic model is that it allows estimation of the approximate degree of enantioselectivity in the bis-cinchona controlled dihydroxylation of an olefinic substrate. Another is the guidance it provides in the design of favorable substrate structures for enantioselective dihydroxylation. These features led to the prediction, and demonstration,

Table 1. Enantioselectivity in the Asymmetric Dihydroxylation of Substrates Possessing Remote Binding Groups Using $(DHQD)_2PYDZ$ (**1**)[8a−c]

Olefin	Product	Yield	% ee
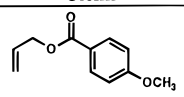	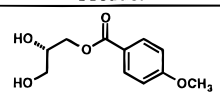	>99%	98%
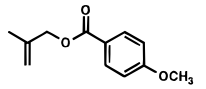	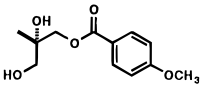	98%	97%
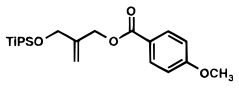	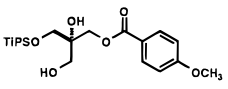	98%	>97%
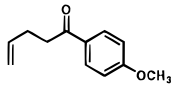	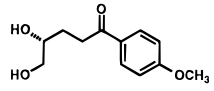	96%	>98%
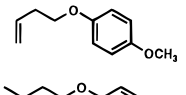	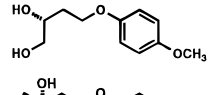	96%	91%
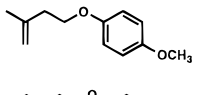	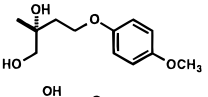	99%	96%
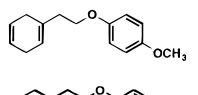	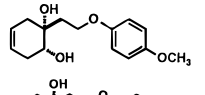	74%	95%
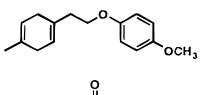	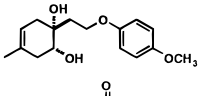	62%	95%
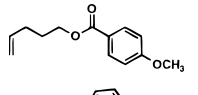	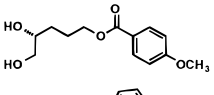	99%	82%
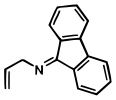	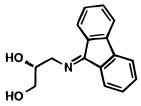	90%	90%

that certain derivatives of terminal allylic alcohols, e.g. 4-methoxybenzoate esters, should undergo dihydroxylation with high enantioselectivity, whereas others, e.g. triisopropylsilyl ethers, should not.[8] The following 4-methoxybenzoates of allylic alcohols were dihydroxylated with the $(DHQD)_2PYDZ-OsO_4$ catalytic system with the indicated product ee's: allyl (98%); 2-methylallyl (97%); (*E*)-crotyl (>99%); 1-cyclohexenylmethyl (98%). (See also Table 1.)[8a] In contrast the observed ee's for the triisopropylsilyl and benzyl ethers of allyl alcohol were 3% and 60%, respectively.[8a] The CCN [3 + 2] model readily accommodates all of the experimental evidence regarding the direction and level of position selectivity and enantioselectivity in these allylic asymmetric dihydroxylations. According to this model, and as shown in Figure 3, allyl 4-methoxybenzoate positions itself such that the 4-methoxybenzoyl ring is interposed between the forward and rearward methoxyquinoline rings of the catalyst, leading to substantial van der Waals binding. With the substrate positioned in this manner, the double bond is

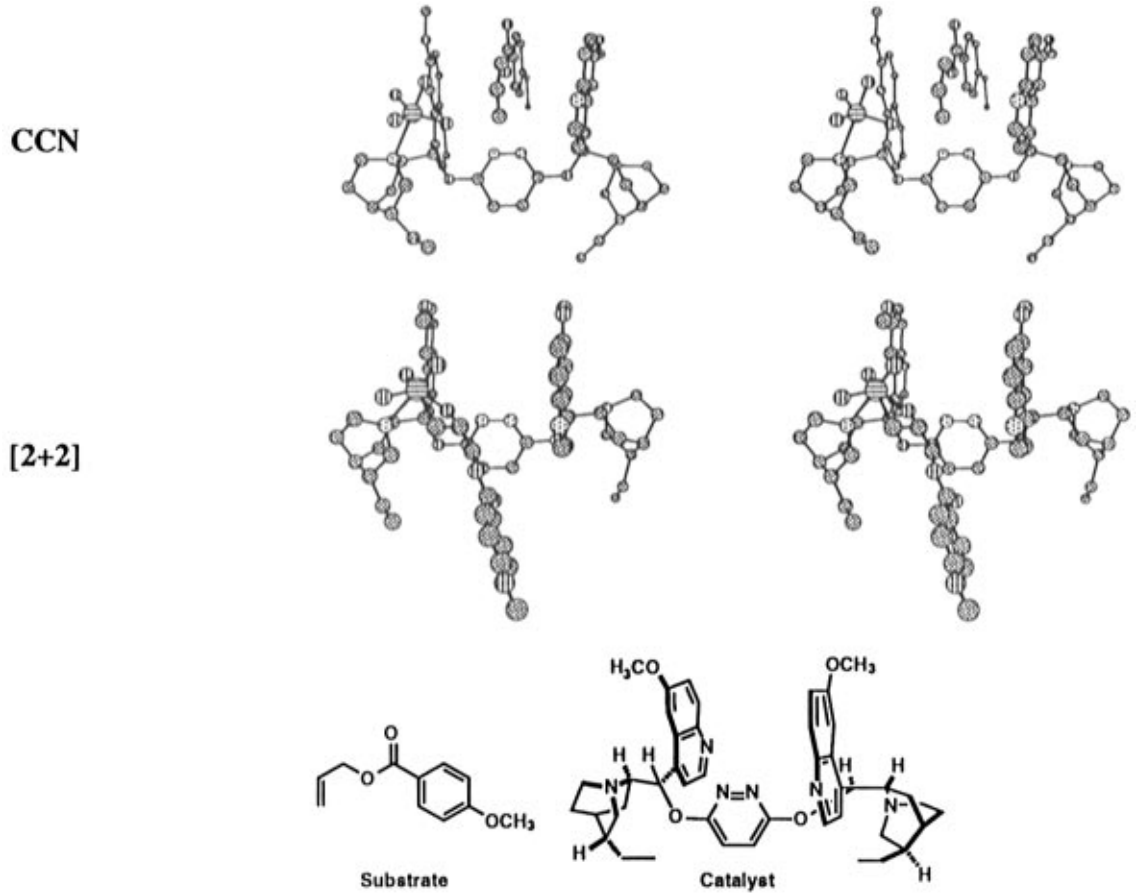

Figure 3. Stereoviews of the two pathways leading to (*S*)-glyceryl-4-methoxybenzoate. Top: [3 + 2] CCN model showing attractive interactions between the substrate 4-methoxybenzoyl group and the U-shaped binding pocket. Bottom: metallaoxetane model.

oriented perfectly for [3 + 2] addition to one axial and one equatorial oxygen of the quinuclidine-bound osmium tetraoxide. The bulky triisopropylsilyl group is too large to fit in the U-shaped binding pocket, and in consequence, allyl triisopropylsilyl ether cannot bind to the catalytic complex as shown in Figure 3. The phenyl ring of allyl benzyl ether prefers to be twisted out of the plane of the double bond, resulting in a less optimum fit in the U-shaped cavity compared to allyl 4-methoxybenzoate.[14]

The metallaoxetane intermediate derived from the [2 + 2] cycloaddition of one Os═O bond to allyl 4-methoxybenzoate is also shown in Figure 3. The ligand−OsO_4 geometry shown for this intermediate corresponds to that used by Sharpless to explain the high levels of enantioselectivity in the dihydroxylation of styrene. In the dihydroxylation of allyl 4-methoxybenzoate, the 4-methoxybenzoyl group is located far beyond the lower edge of the pyridazine spacer group and hence cannot participate in binding interactions with the catalyst L-shaped domain. The lack of binding between the 4-methoxybenzoyl group of the substrate and the cinchona alkaloid catalyst, either in this metallaoxetane or in the diastereomer which produces the enantiomeric diol, implies that the two putative diastereomeric transition states have similar energies and that enantioselectivity would be poor, contrary to fact.

Bishomoallylic 4-methoxybenzoates are predicted to be good substrates for enantioselective dihydroxylation by the [3 + 2] CCN model, whereas homoallylic 4-methoxybenzoates are not. Allylic and bishomoallylic 4-methoxybenzoates, when positioned within the binding pocket in this manner, are both oriented with the ester carbonyl group projecting out the top of the U-shaped pocket toward solvent. For the case of homoallylic ester derivatives, the ester carbonyl group is positioned downward and interacts unfavorably with the nitrogen atoms of the pyridazine ring at the floor of the U-shaped pocket. The important effect of the 4-methoxybenzoyl group in directing position selectivity and enantioselectivity can be clearly understood by means of the CCN [3 + 2] cycloaddition model but not by the metallaoxetane pathway.

The 4-methoxyphenyl ethers of terminal homoallylic alcohols are expected to be good substrates for enantioselective dihydroxylation on the basis of the CCN model. In fact very good enantioselectivities have been demonstrated with a series of homoallylic 4-methoxyphenyl ethers.[8a,b] Table 1 summarizes the data for a number of allylic, homoallylic, and bishomoallylic derivatives. In each case the high level of enantioselectivity and the regioselectivity which are observed agree with the CCN [3 + 2] model, but not with the [2 + 2] model, since the aromatic portion is not involved in the binding domain for the latter.

Further support for the CCN [3 + 2] model for dihydroxylation of bishomoallylic 4-methoxybenzoates derives from the observation that the aromatic group, though remote from the olefinic linkage being oxidized, is held within the U-shaped binding pocket and protrudes through the rear. These facts suggested the study of a catalyst carrying a 9-anthracenylmethyl group on one quinuclidine nitrogen of the $(DHQD)_2PYDZ$ ligand, as shown in Figure 4.[8c] The anthracenyl group, whose size causes it to adopt the conformation shown in Figure 4, provides another contact area for bishomoallylic 4-methoxybenzoates near the rear of the U-shaped binding pocket of the

(14) For conformational preferences of benzylic systems, see: Smith, H. E.; Fontana L. P. *J. Org. Chem.* **1991**, *56*, 432 and references cited therein.

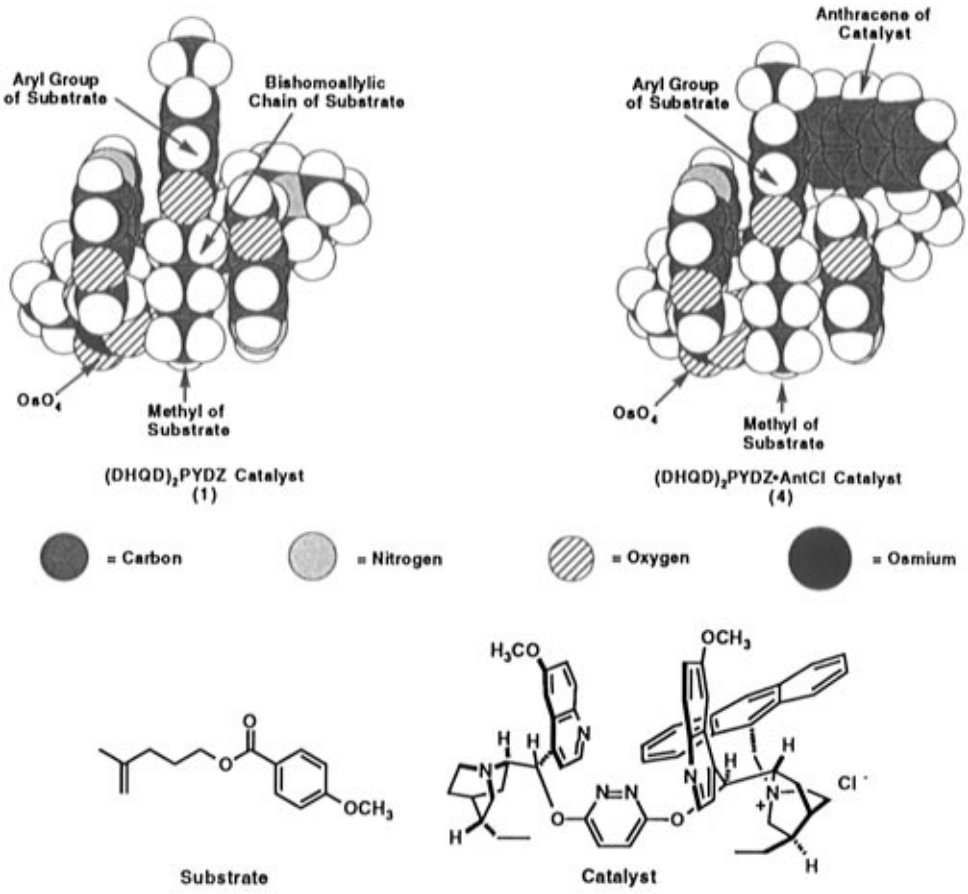

Figure 4. Proposed transition state geometries for the catalytic asymmetric dihydroxylation of bishomoallylic 4-methoxybenzoates using the biscinchona alkaloid catalysts **1** and **4**.

catalyst. As expected from the CCN model, terminal bishomoallylic 4-methoxybenzoates are dihydroxylated with significantly better enantioselectivity using the ligand **4** as compared to $(DHQD)_2PYDZ$, which lacks the 9-anthracenylmethyl group. This observation conflicts with the [2 + 2] model since the 9-anthracenylmethyl group in that model should provide no additional transition state stabilization because it is totally remote from the substrate. In contrast, the role of the 9-anthracenylmethyl group in stabilizing the transition state for the enantioselective dihydroxylation of these substrates follows clearly from the CCN model for enantioselective [3 + 2] cycloaddition. Thus, with the substrate positioned within the U-shaped binding pocket as shown in Figure 4, the anthracenyl group of **4** is oriented so as to allow additional aryl−aryl stacking type van der Waals interactions between the catalyst and the 4-methoxybenzoyl group of the substrate which lower the free energy of the transition state for enantioselective dihydroxylation.

Substrates Possessing Extended Polycyclic Aromatic Binding Groups. The proposed binding domains for the [3 + 2] and [2 + 2] cycloaddition pathways possess such different topology that the two mechanisms can be differentiated by the judicious selection of test substrates. We described in the preceding section a number of highly enantioselective dihydroxylations of terminal olefins which are not expected on the basis of the Sharpless metallaoxetane model due to the absence of substantial binding between the substrate and the putative L-shaped binding region. This section and that which follows describe experiments on another series of highly enantioselective dihydroxylations involving polycyclic substrates which are too large to fit the L-shaped pocket proposed in the Sharpless model.

While the U-shaped pocket of the CCN model can accommodate substrates with extended aromatic groups due to its open ceiling, the Sharpless L-shaped binding domain, which presents an aromatic wall 5.5 Å to the right of the quinuclidine-bound OsO_4, cannot. Thus, substrates possessing large aromatic groups coplanar with the double bond lead to [2 + 2] adducts which overrun the L-shaped pocket. Results with a number of such test substrates are summarized in Table 2. The absolute configurations of the diols derived from **7**, **8**, and **10** have been rigorously established by X-ray crystallographic analysis of appropriate heavy atom derivatives.[15] Specific interactions between one representative substrate (**8**) and each of the proposed catalytic pockets will be discussed below. A stereopair representation of the catalyst−olefin complex for the dihydroxylation of this substrate based on each of the mechanistic models is shown in Figure 5. The metallaoxetane binding geometry in each case parallels that proposed for styrene as shown in Figure 2.

Each of the substrates shown in Table 2 possesses a long aromatic group that cannot fit within the Sharpless L-shaped region. Thus, the metallaoxetane intermediate shown in Figure 5 is prohibitively destabilized by enormous steric repulsion between the fluorenyl group and the forward (right) methoxyquinoline wall of the catalyst, with minimal binding between one portion of the fluorenyl group of **8** and the pyridazine spacer of the catalyst. Similar destabilization can be expected for metallaoxetanes derived from the other substrates in Table 2, especially for the case of **10**, for which the anthracene ring would run through both the forward methoxyquinoline wall and the quinuclidine ring of the catalyst. The Sharpless mechanism

(15) Detailed X-ray crystallographic data are obtainable from the Cambridge Crystallographic Data Center, 12 Union Road, Cambridge, CB2 1EZ, U.K.

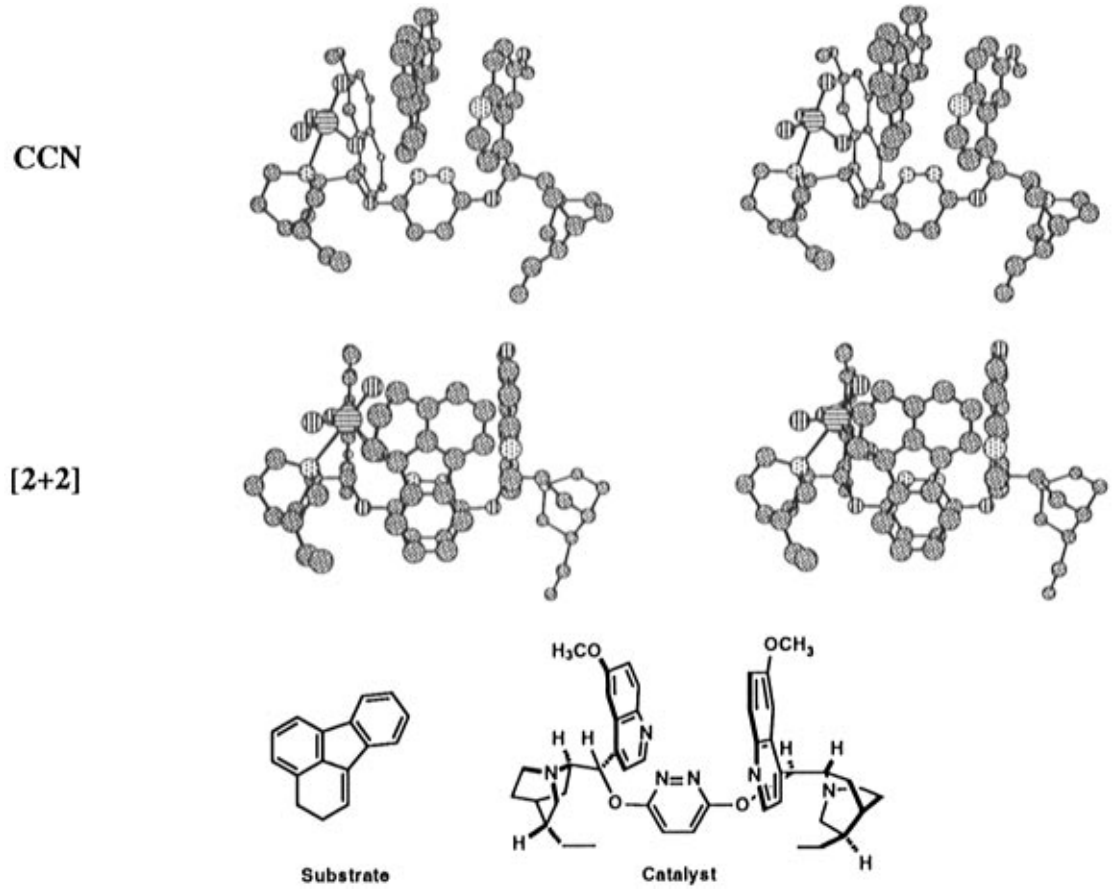

Figure 5. Stereoview of two possible pathways leading to the observed enantiomer of the diol derived from **8**. Top: [3 + 2] addition model showing the favorable interactions between the substrate fluorene ring and the catalyst U-shaped pocket. Bottom: metallaoxetane intermediate.

Table 2. Enantioselectivity in the Asymmetric Dihydroxylation of Olefins Possessing Extended, Planar Binding Groups Using the $(DHQD)_2PYDZ$ Ligand (**1**)

Olefin	Structure	Product	Yield	% ee
5		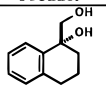	90%	94%
6	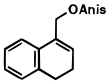	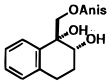	32%	98%
7	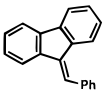	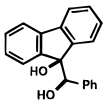	61%	97%
8	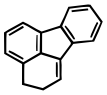	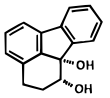	91%	95%
9	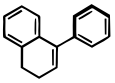	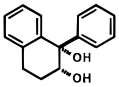	79%	77%
10	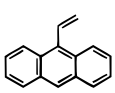	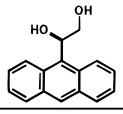	75%	>98%

predicts either the predominance of that enantiomer which is formed only in minuscule proportion, or no selectivity at all.

The CCN [3 + 2] cycloaddition pathway provides a clear and simple explanation for all of the observed enantioselectivities in Table 2. The transition state assembly for the asymmetric dihydroxylation of **8** using the $(DHQD)_2PYDZ{\cdot}OsO_4$ catalyst appears in Figure 5. This catalyst−substrate complex geometry parallels that shown for the asymmetric dihydroxylation of styrene in Figure 1. The fluorenyl ring of the substrate nestles comfortably within the U-shaped pocket of the catalyst. In this geometry, the double bond of the substrate is positioned perfectly for the [3 + 2] cycloaddition that produces the observed enantiomer of the diol. A similar analysis can be used to understand enantioselectivity in the dihydroxylation of **7**. With the fluorenyl ring of this substrate positioned in the U-shaped pocket of the catalyst, the isolated phenyl ring of the substrate lies over the catalyst pyridazine linker group. Binding energy for the catalyst−substrate complex is derived from aryl−aryl stacking and van der Waals interaction of each aromatic ring of the substrate and the individual aromatic rings of the U-shaped cavity. Dihydroxylation of the opposite olefin face as that shown in Figure 5 is suppressed by severe steric repulsion which would result from positioning the substrate aromatic groups close to the pyridazine linker. Unlike the Sharpless L-shaped pocket, the U-shaped region of the catalyst, which provides most of the transition state stabilizing binding, accommodates the extended aromatic group of the substrate without concomitant repulsion.

A similar CCN analysis can be applied successfully to the other examples shown in Table 2. Dihydrofluoranthene (**8**) is dihydroxylated with high enantioselectivity by the ligand **1**, as expected. However, considerably lower selectivity is observed in the reaction of **9**. The reduced enantioselectivity for **9** as compared to **8** is readily understood by the CCN model in terms of the nonplanarity of the phenyl substituent in **9** with the olefinic linkage. Such non planarity reduces binding within the U-shaped pocket. The anthracenyl ring of **10** and the double bond are nonplanar, but unlike substrate **9**, which possesses two different aromatic rings that can be held within the U-shaped pocket and thereby produce enantiomeric diols, **10** possesses

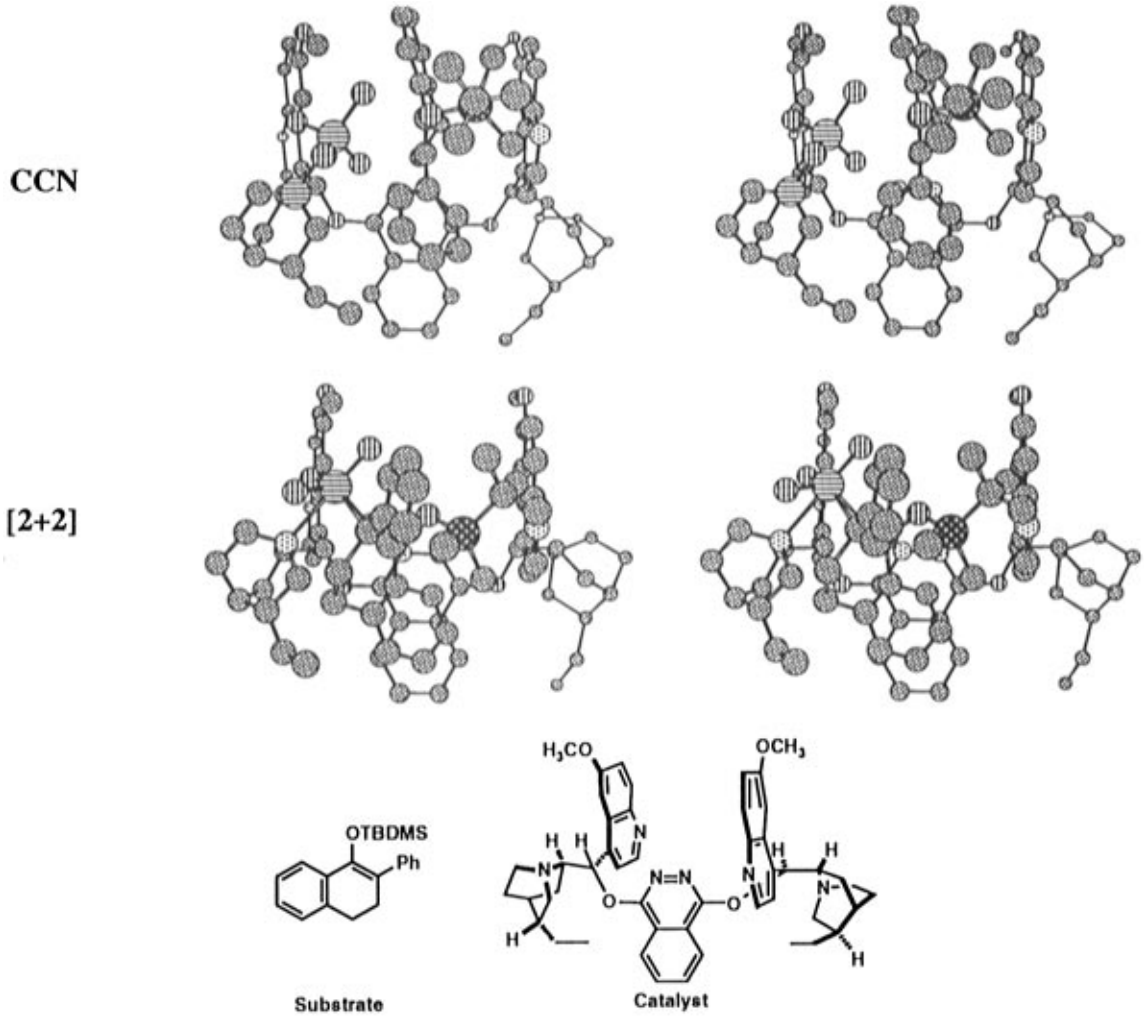

Figure 6. Stereoviews of the two pathways for the asymmetric dihydroxylation of **11**. Top: [3 + 2] addition pathway showing attractive interactions between the substrate aryl groups and the catalyst U-shaped pocket. Bottom: metallaoxetane intermediate.

only one aromatic binding group. Association of that group with the U-shaped pocket results in highly enantioselective catalytic dihydroxylation.

Tetrasubstituted Olefins. Enantioselectivity in the Sharpless asymmetric dihydroxylation is highest for terminal, 1,1-disubstituted, (*E*)-1,2-disubstituted, and trisubstituted olefins. The asymmetric dihydroxylation of tetrasubstituted olefins has recently been developed using electron-rich substrates and increased catalyst loading.[16] Catalysts for the dihydroxylation of these olefins turn over very slowly as a result of steric factors that impede the hydrolysis of the intermediate osmium(VI) esters. Tetrasubstituted olefins which are dihydroxylated with high enantioselectivity (>90%) possess aromatic groups as well as coplanar endocyclic double bonds. The highly enantioselective dihydroxylation of these substrates provides further evidence in favor of a [3 + 2] pathway. A typical example is shown in Figure 6, a stereopair representation of the [3 + 2] and [2 + 2] structures corresponding to the preferred asymmetric dihydroxylation of **11**. Several analogous examples appear in Table 3.

The metallaoxetane intermediates for the asymmetric dihydroxylation of each of these substrates are subject to a prohibitive level of steric repulsion between the substrate and the catalyst, as is revealed in Figure 6. These unfavorable interactions arise as a result of the proximity of the substrate to both the quinuclidine ring and the distal methoxyquinoline ring (right side). This type of repulsion has been associated with the *unfavorable pathway* (i.e. leading to the minor enantiomer) in the asymmetric dihydroxylation of (*E*)-1,2-disubstituted and trisubstituted olefins.[9d] It has also been used to explain the poor enantioselectivity generally observed in the dihydroxylation of (*Z*)-1,2-disubstituted olefins.[9d] For tetrasubstituted olefins, however, one substituent is required to occupy this disfavored position in the metallaoxetane intermediate. For this reason, Sharpless has incorporated the proviso that, for tetrasubstituted olefins, the metallaoxetane structure does not even exist as a reaction intermediate, but occurs as a transition state for the dihydroxylation.[9] Indeed, the Sharpless metallaoxetane model does not explain the high enantioselectivities observed for any of the dihydroxylation reactions of the tetrasubstituted olefins shown in Table 3. In contrast, the direction and level of

Table 3. Enantioselectivity in the Asymmetric Dihydroxylation of Tetrasubstituted Olefins Using the $(DHQD)_2PHAL$ Ligand[14]

Olefin	Structure	Product	Yield	% ee
11	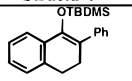	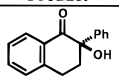	94-98%	93%
12	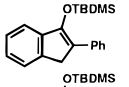	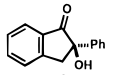	23-32%	89%
13	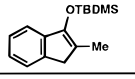	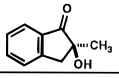	64-85%	85%

(16) Morikawa, K.; Park, J.; Andersson, P. G.; Hashiyama, T.; Sharpless, K. B. *J. Am. Chem. Soc.* **1993**, *115*, 8463.

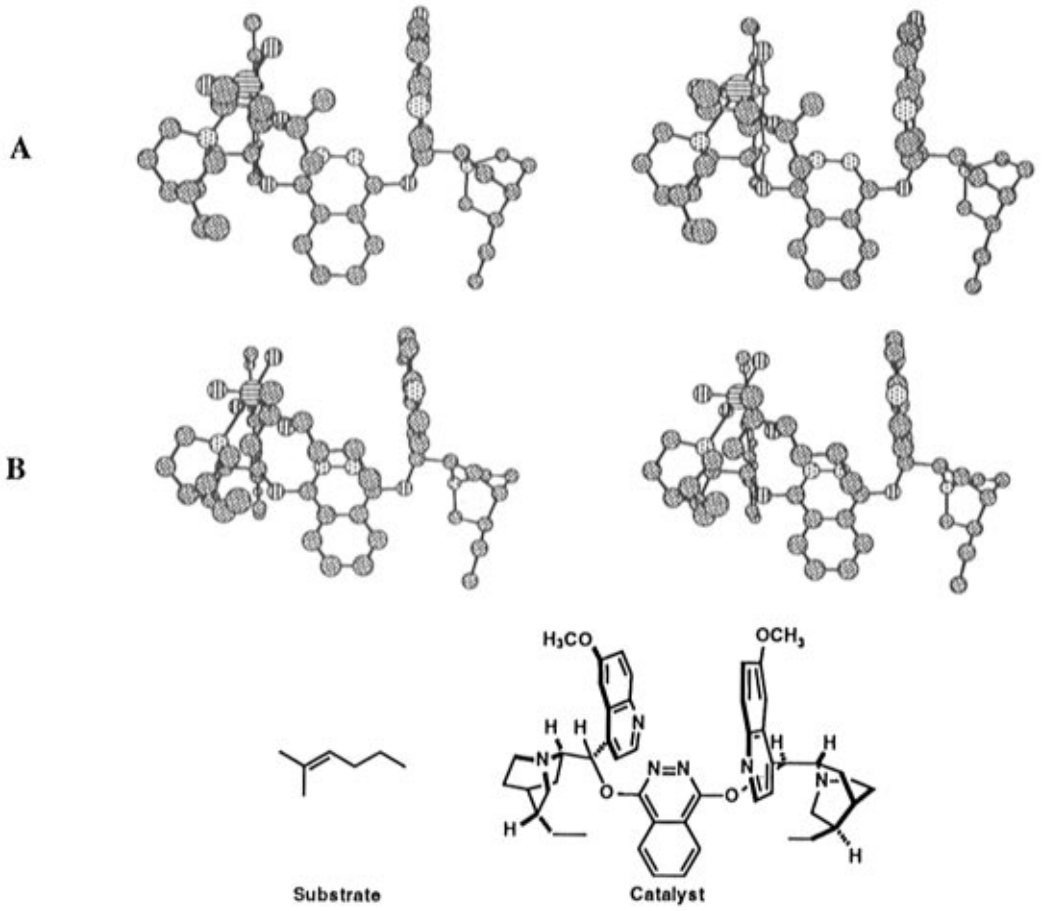

Figure 7. The two possible metallaoxetane intermediates that lead to the observed enantiomer of the diol derived from **14**. The lower intermediate is disfavored due to repulsive interactions between one substrate methyl group and the catalyst quinuclidine ring.

enantioselectivity observed in these oxidations is well explained by the [3 + 2] model. The necessity for an endocyclic double bond in the substrate follows from the requirement that steric repulsions between the endocyclic methylene groups of the substrate and the pyridazine spacer of the catalyst be minimized. Thus, with the fused aromatic ring held within the binding region of the catalyst, the double bond of **11** is positioned perfectly for oxidation to the observed enantiomer of the product. This geometry of the catalyst−substrate complex does not impose unfavorable steric repulsion on the transition state for dihydroxylation, since the binding pocket accommodates the crucial substrate domain (see Figure 6) and the silyl group of the substrate projects forward of the pocket. Dihydroxylation of the opposite face of the double bond is disfavored by repulsive interactions involving the catalyst linker group and the phenyl substituent of **11** and between the silyl group of the substrate and the U-shaped binding pocket. The simplicity of the argument for enantioselectivity in the asymmetric dihydroxylation of these substrates using this CCN model contrasts with the lack of agreement with the Sharpless metallaoxetane model.

Trisubstituted Olefins. Trisubstituted olefins generally are dihydroxylated with high levels of enantioselectivity, and this observation can be understood in terms of prohibitive steric interactions between the substrate and the catalyst in the transition state for formation of the disfavored enantiomer. While both models offer a qualitative understanding of the direction of enantioselectivity in these reactions, the CCN model better accounts for the stabilizing interactions between the substrate and the catalyst that are crucial for high enantioselectivity. As shown in Figure 7, two isomeric metallaoxetane intermediates are possible for the formation of the favored enantiomeric diol derived from the oxidation of 2-methylhex-2-ene, Markovnikov (A) and non-Markovnikov (B). Although it is conceivable that both the Markovnikov and non-Markovnikov intermediates are formed easily, neither type of transition state involves binding of the long aliphatic chain of any of the substrates shown in Table 4 while at the same time avoiding an unfavorable steric interaction between the *cis*-vinylic substituent and the quinuclidine ring of the catalyst. In the case of substrates **15** and **17** the [2 + 2] transition state suffers from steric repulsion between the silyl group of the substrate and the distal (right) methoxyquinoline ring of the catalyst. The minimal contact between the substrate and the L-shaped catalytic pocket in the geometry shown in Figure 7A combined with the significant steric

Table 4. Enantioselectivity in the Asymmetric Dihydroxylation of Trisubstituted Olefins Using the $(DHQD)_2PHAL$ Ligand[3]

Entry	Substrate	Product	Yield	% ee
14	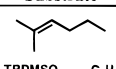		-	98%
15	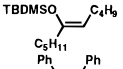		68-95%	89%
16	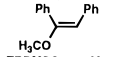		68-95%	90%
17	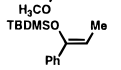		68-95%	97%
18	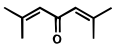	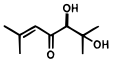	59%	89%
19	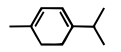		78%	86%
20	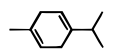		84%	96%
21	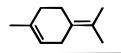		80%	92%

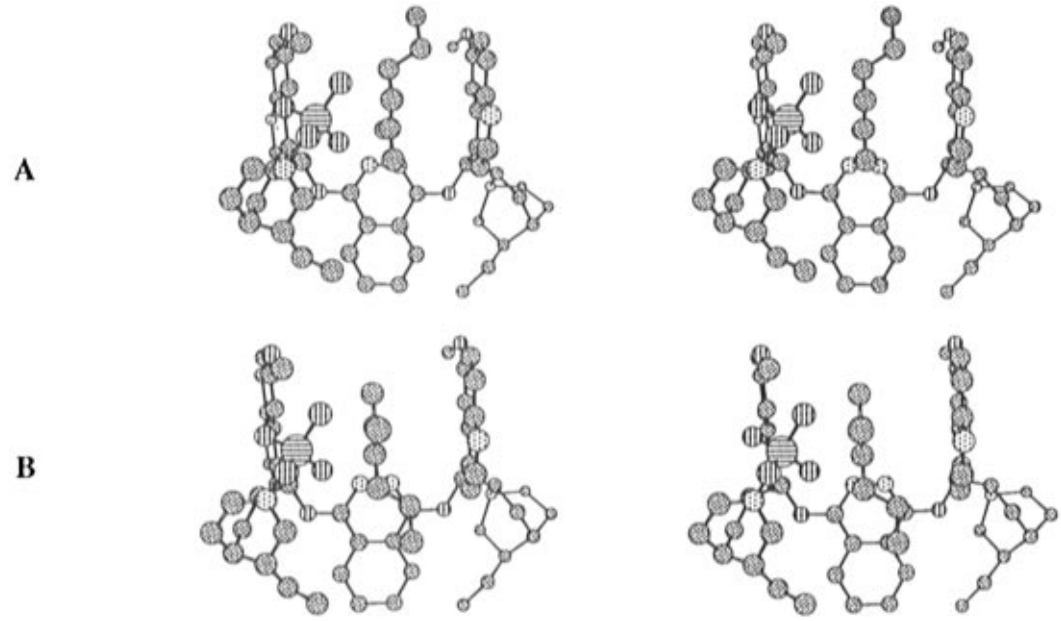

Figure 8. The two possible substrate−catalyst complexes that lead to the observed enantiomer of the diol derived from **14** *via* the [3 + 2] addition pathway. The upper complex is less favorable due to steric interactions between a substrate methyl group and the catalyst pyridazine linker.

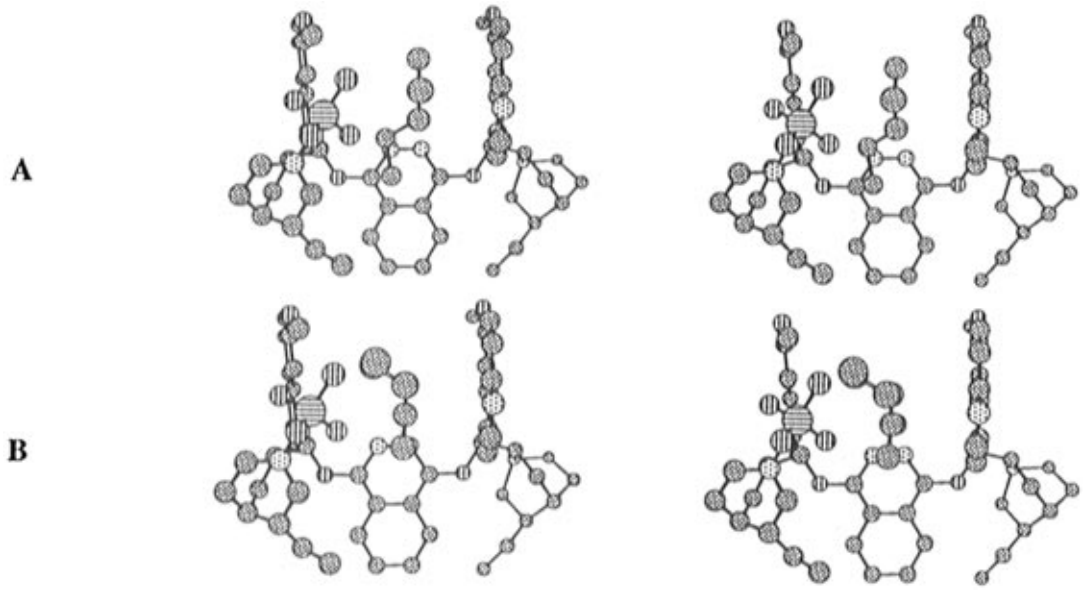

Figure 9. The two possible substrate−catalyst complexes that lead to the minor enantiomer of the diol derived from **14** *via* the [3 + 2] addition pathway. The complex shown in A suffers from severe steric repulsions between the propyl group of the substrate and the phthalazine linker of the catalyst. The complex shown in B is less favorable than the pathway shown in Figure 8B due to steric repulsion of one of the substrate methyl groups and the phthalazine spacer of the catalyst.

interactions that disfavor dihydroxylation through the intermediate shown in Figure 7B suggest that other oxidation pathways would compete with those shown in Figure 7 (that lead to the observed enantiomer) with loss of enantioselectivity. The highly enantioselective dihydroxylations of the substrates shown in Table 4 are not expected from the Sharpless model.

The [3 + 2] cycloaddition model, on the other hand, provides a simple rationale for the observed enantioselectivities in the dihydroxylation of these substrates. Two possible transition state arrangements for the production of the observed diol enantiomer are shown in Figure 8. These differ by a 180° rotation about a horizontal line in the plane of the page and through the center of the double bond. In the structure in Figure 8A, the aliphatic chain is positioned within the U-shaped pocket, while the *cis*-methyl group lies close to the phthalazine spacer group of the catalyst, probably resulting in some steric repulsion between these groups. In the structure shown in Figure 8B, the aliphatic chain of the substrate makes van der Waals contact with the phthalazine spacer while the isopropylidene group binds to the forward (right) methoxyquinoline ring. This is the more favorable of the two possible arrangements which lead to the preferred product. The two analogous structures which lie on the pathway to the disfavored enantiomeric diol involve severe repulsions as shown in Figure 9. A similar analysis explains each of the other cases summarized in Table 4. The CCN model has also been used to design catalysts for the highly position selective and enantioselective dihydroxylation of oligoterpene derivatives using modified cinchona alkaloid derivatives that possess (1) extended aromatic linker groups (to increase binding of the substrate) and (2) branched O6′ groups (to block deep penetration of the substrate into the U-shaped binding pocket) (*vide infra*).

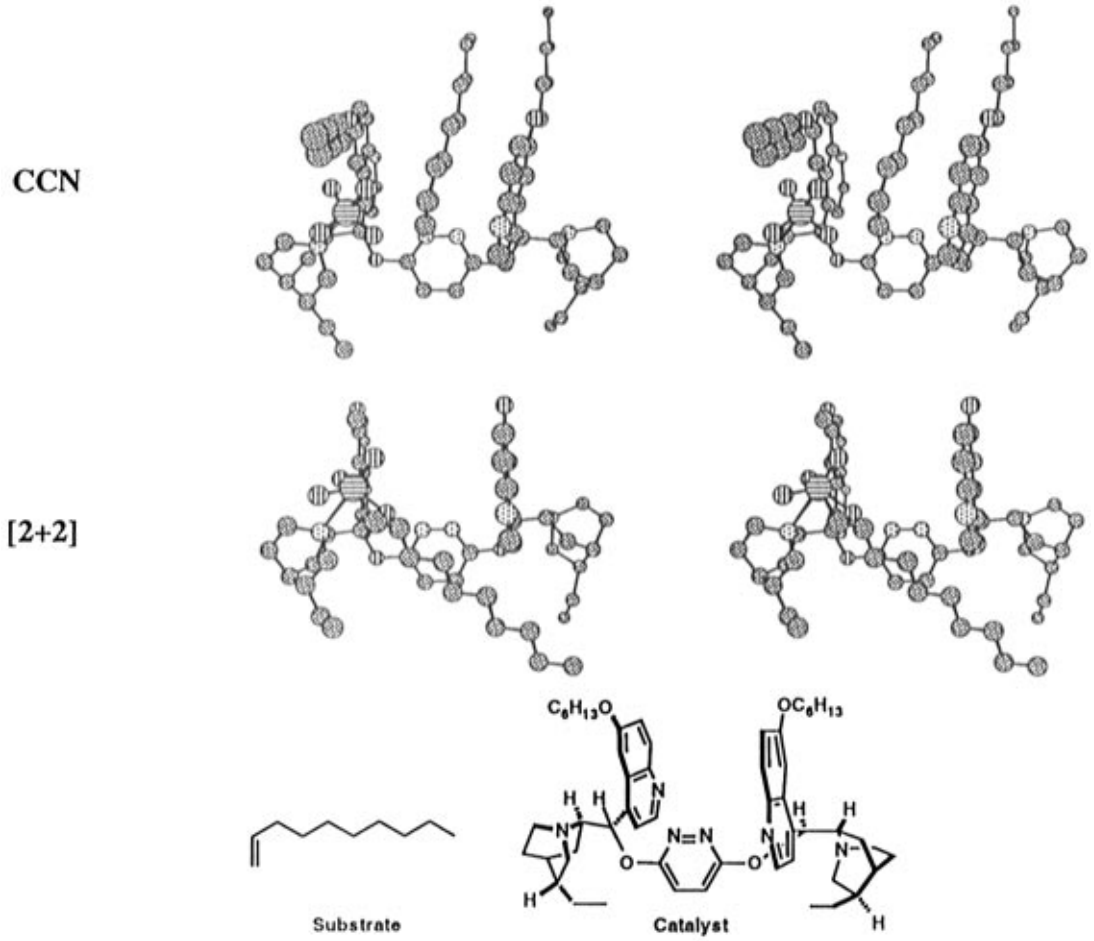

Figure 10. Stereoviews of the two pathways for the asymmetric dihydroxylation of decene showing the potential effects of catalyst O6′ substitution. Top: [3 + 2] addition pathway for the asymmetric dihydroxylation catalyzed by 3,6-bis(O6′-hexylhydrocupreidyl)pyridazine. Bottom: metallaoxetane intermediate for the dihydroxylation catalyzed by **1**.

Catalyst Structure and Enantioselectivity. In the foregoing section on the description of the CCN and Sharpless mechanistic models, it was pointed out that for the Sharpless [2 + 2] transition state, the most important contact area for van der Waals binding between the substrate and the catalyst is the flat bicyclic phthalazine spacer which links the two cinchona subunits. Consequently, one would expect that the replacement of the phthalazine fused ring system by a single pyridazine ring would produce sizable changes in enantioselectivity since the binding between the substrate and linker would be substantially reduced. We have determined the enantioselectivities for the catalytic dihydroxylation of a series of nine different olefins with both $(DHQD)_2PHAL$ and $(DHQD)_2PYDZ$ ligands at 0 °C using the standard procedure described in the experimental section. The experimental data which are summarized in Table 5 show that the use of $(DHQD)_2PHAL$ and $(DHQD)_2PYDZ$ ligands leads to essentially identical enantioselectivities with this structurally diverse set of substrates.[17] This result accords best with the CCN model which involves similar contact binding areas in the transition state between the substrate and the phthalazine or pyridazine linker. In the CCN model, van der Waals binding between the olefinic substrate and the U-shaped binding pocket (the methoxyquinoline subunits) is very important, and the principal contact between the substrate and catalyst at the bottom of the U-pocket is with the two ring nitrogens of the pyridazine or phthalazine spacer.

Table 5. Comparison of Enantioselectivities Obtained in the Asymmetric Dihydroxylation of Olefins at 0 °C Using the $(DHQD)_2PHAL$ (PHAL) and $(DHQD)_2PYDZ$ (PYDZ) Ligands

Olefin	Product	% ee (PYDZ)	% ee (PHAL)
	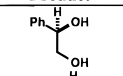	96%	97%
	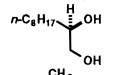	83%	84%
	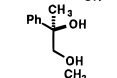	93%	94%
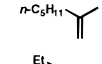	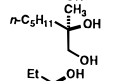	65%	66%
	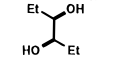	93%	93%
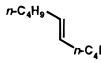	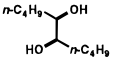	96%	97%
	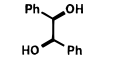	>98%	>98%
	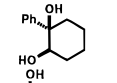	98%	98%
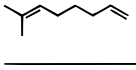	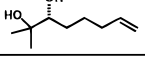	95%	98%

The fact that the Sharpless model implies only a minor binding interaction between the [2 + 2] bound substrate and one of the methoxyquinoline rings (right side, distal to OsO_4) implies that there should be no role of the 6′-methoxy substituents on the quinoline rings in substrate binding. In contrast,

(17) For comparisons of the $(DHQD)_2PYDZ$ and $(DHQD)_2PHAL$ ligands, see: (a) Crispino, G. A.; Makita, A.; Wang, Z.-M.; Sharpless, K. B. *Tetrahedron Lett.* **1994**, *35*, 543. (b) Reference 7e.

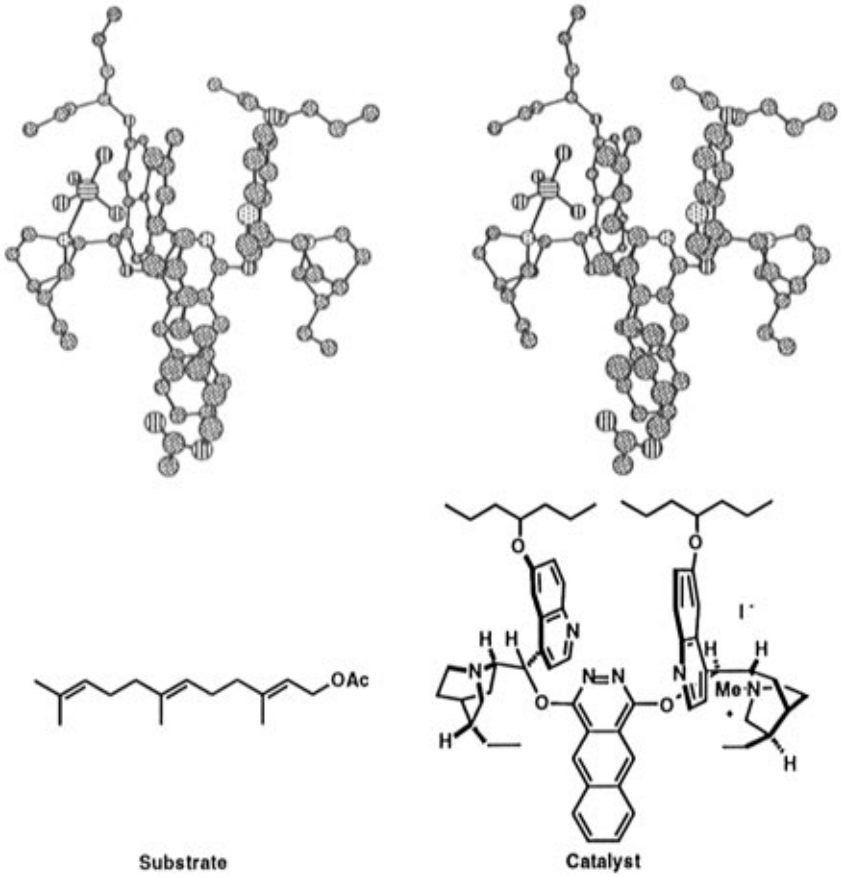

Figure 11. Stereoview of the proposed transition state arrangement for the position-selective dihydroxylation of farnesyl acetate using the O6′-4-heptyl analog of **1**. The methyl iodide group has been omitted from the stereoview for clarity.

the CCN [3 + 2] model intimately involves both of the 6′-alkoxy substituents in binding to that portion of the substrate which lies within the two sides of the U-shaped binding region. Figure 10 illustrates the binding expected for 1-decene as substrate according to the CCN and Sharpless models. As described previously for the dihydroxylation of styrene, the 6′-substituent on the quinoline rings has an important effect on enantioselectivity.[7a,18] In the dihydroxylation of styrene, for example, the observed enantiomeric excess of the product diol as a function of the 6′-substituent X of similar size is as follows: X = OMe, 96%; X = CH_2Me, 93%; X = O-*n*-Bu, 97%. However, for the smaller group X = H, the observed ee was only 82% and for the larger X = O-triisopropylsilyl, only 50%. These results are not expected from the Sharpless model, but they can readily be understood from the CCN model.

The CCN model also has allowed the design of catalysts which close off the rear of the U-shaped binding pocket with concomitant limits on the degree with which a substrate can penetrate the U-domain. These considerations have led to the synthesis of the O6′-4-heptyl analog of the $(DHQD)_2$ ligand with a benzophthalazine linker and the demonstration that this ligand leads to very high position selectivity in the dihydroxylation of di-, tri-, and polyolefinic substrates.[8d] The CCN transition state for the dihydroxylation at the distal double bond of farnesyl acetate (selectivity >120:1) is shown in Figure 11. This high position selectivity was correctly predicted in advance by the CCN model. We are not aware of any [2 + 2] type transition state proposals which explain position selectivity in the dihydroxylation of polyenes.

Another type of cinchona-based catalytic system which tests the mechanistic models for OsO_4-mediated bishydroxylation is that represented by the two diastereomeric mono-DHQD-mono-1-anthracenyl ligands **22** and **23**.[7c] As shown in the formula, ligand **23** presents a binding pocket which projects rearward of the pyridazine ring. Although this catalytic ligand is inferior to **1** for the asymmetric dihydroxylation of substrates such as styrene, olefins possessing extended binding groups are dihydroxylated with high enantioselectivity (see Table 6). Thus, the allylic 4-methoxybenzoates and 2-vinylnaphthalene are good substrates for the asymmetric dihydroxylation using this catalyst. These results can be readily understood in terms of the U-shaped binding pocket proposed in the CCN model, as the extended aromatic group projects far enough from the double bond to

Table 6. Enantioselectivity in the Asymmetric Dihydroxylation of Olefins Using DHQD−PYDZ−Anthracenyl Ligands[7c,8e]

Entry	Olefin	1, ee, (% yield)	22, ee, (% yield)	23, ee, (% yield)
1		> 99 (99)	> 98 (92)	98 (96)
2		93 (58)	96 (74)	78 (46)
3		96 (95)	91 (76)	80 (82)
4	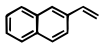	99 (98)	98 (93)	91 (99)
5	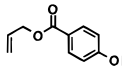	98 (>99)	95 (>99)	90 (98)
6	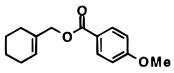	98 (>99)	98 (>99)	95 (>99)
7		79 (95)	78 (86)	44 (99)
8		98 (88)	93 (99)	90 (99)

(18) Arrington, M. P.; Bennani, Y. L.; Göbel, T.; Walsh, P.; Zhao, S.-H.; Sharpless, K. B. *Tetrahedron Lett.* **1993**, *34*, 7375.

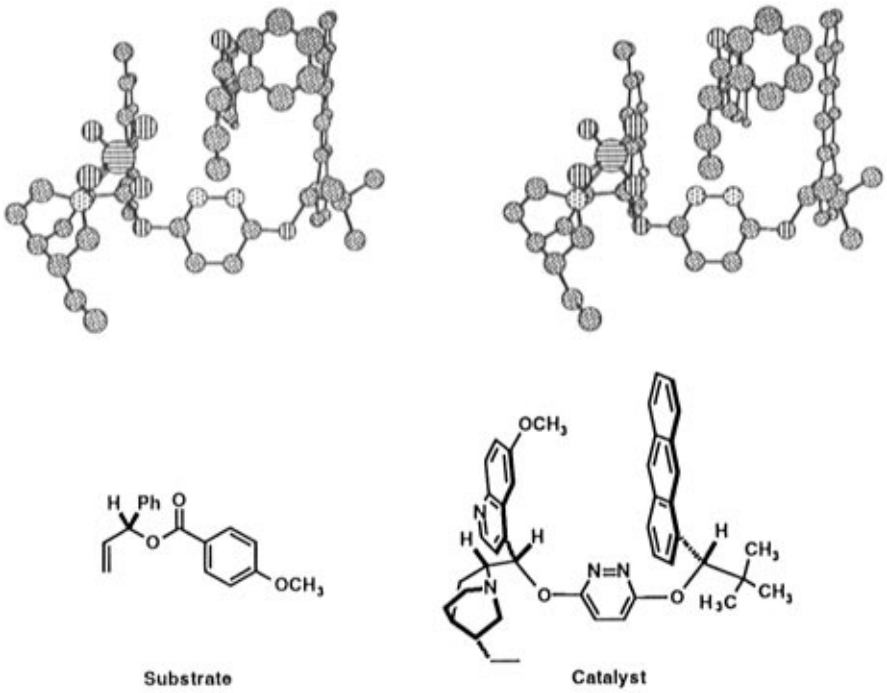

Figure 12. Stereoview of the proposed transition state arrangement for the asymmetric dihydroxylation of (*S*)-phenyl-2-propen-1-yl 4-methoxybenzoate catalyzed by **23**.

interact with the remotely located binding pocket. The slightly lower enantioselectivity that results from the use of catalyst ligand **23** as compared to **1** or **22** can be understood in terms of the loss of favorable contacts between the substrate vinyl group and the catalyst on displacement of the forward aromatic ring of the catalyst to the rear of the binding region. Most of the binding between substrate and catalyst in the transition state is the result of aromatic stacking interactions between the remote binding group of the substrate and the rearward portion of the catalyst U-shaped pocket.

The Sharpless metallaoxetane model seems inconsistent with the data in Table 6. According to the Sharpless model, the distal (right side) quinoline ring provides only a modest edge−face aromatic interaction with styrene in the metallaoxetane intermediate, as shown in Figure 2. Close examination of this drawing reveals minimal contacts between the substrate and the methoxyquinoline wall that forms half of the proposed L-shaped domain. It would be expected from this model that replacement of the second alkaloid moiety with a methoxy group would only slightly affect enantioselectivity. This expectation is contrary to experimental results, as this replacement results in a catastrophic deterioration in enantioselectivity.[7e] If the forward methoxyquinoline ring provides crucial binding interactions with the substrate, then it is also not clear why catalyst **23**, which lacks a forward aromatic group, provides excellent enantioselectivity in the asymmetric dihydroxylation of substrates that possess remote binding groups.

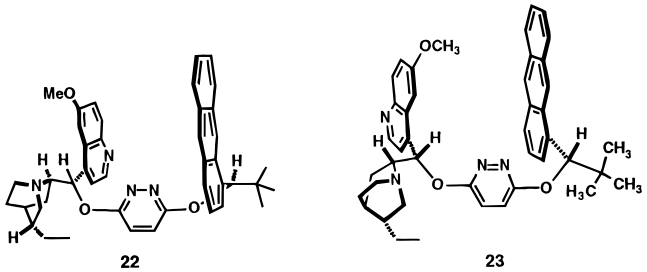

Kinetic Resolution of Racemic Substrates. The CCN mechanistic model has provided such a detailed picture of the transition state for bis-cinchona-catalyzed enantioselective dihydroxylation of olefins that a number of subtle and powerful new applications have been developed under its guidance. One such advance stemmed from the expectation that the kinetic resolution of the 4-methoxybenzoates of racemic allylic alcohols with chirality about C(1) should be feasible. The experimental verification of this prediction has recently been described in detail.[8e] The salient results are summarized in Table 7, which documents the unprecedented effectiveness of this approach for a number of racemic substrates. A stereopair representation of the proposed pathway for the dihydroxylation of the more rapidly dihydroxylated enantiomer (*S*)-**24** appears in Figure 12 with the results for the process shown in Table 7. The excellent structural complementarity of the catalyst and the substrate provides a clear basis for understanding the scope, level, and direction of the kinetic resolution. In the CCN transition state for the dihydroxylation of (*S*)-**24**, the olefinic carbons are correctly aligned for [3 + 2] cycloaddition with one axial and

Table 7. Kinetic Resolution of Racemic Allylic 4-Methoxybenzoates Using Cinchona Alkaloid Ligands

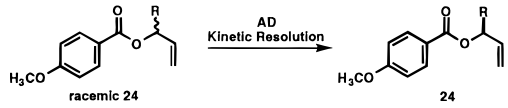

Substrate	Ligand	k_{rel}[a]
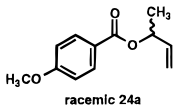 racemic 24a	$(DHQD)_2PYDZ$ (1)	3.1
	DHQD-PYDZ-(*S*)-anthryl (23)	20
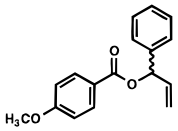 racemic 24b	$(DHQD)_2PYDZ$ (1)	1.9
	DHQD-PYDZ-(*S*)-anthryl (23)	79

[a] Relative rates of reaction of ent-**24** and **24**.

one equatorial oxygen of complexed OsO_4, and the 4-methoxybenzoate subunit is correctly positioned for good binding in the U-shaped domain, while the phenyl substituent is located so as to avoid any unfavorable nonbonded steric interaction. Indeed, there is a van der Waals binding contact between the face of the phenyl group and the front edge of the anthracene ring on the right side of the U-domain. The (*R*)-enantiomer of 1-phenyl-2-propen-1-yl 4-methoxybenzoate cannot bind in a way analogous to the (*S*)-enantiomer binding shown in Figure 12 because of large steric repulsion between the phenyl group and the left wall of the U-shaped domain (including the coordinated OsO_4). As expected from the CCN mechanistic model, the effectiveness of the kinetic resolution process decreases when the phenyl substituent at C(1) of the racemic allylic ester is replaced by the smaller methyl group (Table 7).

Summary and Conclusions

The determination of the fine mechanistic details of important new enantioselective processes represents a major challenge to chemists, and also a great opportunity, since the detailed understanding of mechanism can reveal important new principles for further discovery. In the present analysis, the evidence on the mechanism of the bis-cinchona alkaloid catalyzed enantioselective dihydroxylation has been examined as broadly as possible in order to distinguish between [2 + 2] cycloaddition (Sharpless) and [3 + 2] cycloaddition (CCN; see Figure 1) models. The following lines of evidence have been found to support the CCN model: (1) enantioselectivity as a function of olefin structure for a wide range of olefinic substrates, (2) enantioselectivity as a function of catalyst structure for a variety of catalysts in the cinchona series, and (3) observed Michaelis−Menten kinetics which demonstrate rapid reversible formation of an intermediate prior to the rate-limiting step.[19] We know of no experimental evidence which is not in accord with the CCN model.

The value and utility of any mechanistic model reside in its predictive power and its ability to lead to successful new applications. In addition to being consistent with all the experimental observations, the CCN model has led to numerous improvements in enantioselectivity in the asymmetric dihydroxylation of substrates that initially failed in this reaction. Some novel applications that have broader impact on organic synthesis have also been discovered through the logical application of the [3 + 2] model; for example, (1) position selective terminal dihydroxylation of oligoterpene derivatives, (2) position selective dihydroxylation of allylic 4-methoxybenzoates and related analogs that allow multiple double bonds to be oxidatively differentiated by means of a removable directing group, and (3) kinetic resolution of racemic allylic 4-methoxybenzoates that has powerful implications for the desymmetrization of prochiral substrates.

Experimental Section

1-[[(4-Methoxybenzoyl)oxy]methyl]-3,4-dihydronaphthalene (6). 1-(Hydroxymethyl)-3,4-dihydronaphthalene[20] was converted to **6** using the previously reported general procedure for the preparation of allylic 4-methoxybenzoates:[8a] R_f = 0.35 (15:85 ethyl acetate−hexane); ^{1}H NMR ($CDCl_3$, 400 MHz) δ 8.01 (m, 2H), 7.33 (m, 1H), 7.23−7.17 (m, 3H), 6.90 (m, 2H), 6.27 (t, 1H, J = 4.5 Hz), 5.17 (d, 2H, J = 1.1 Hz), 3.85 (s, 3H), 2.83 (t, 2H, J = 8.1 Hz), 2.38 (m, 2H) ppm; ^{13}C NMR ($CDCl_3$, 100 MHz) δ 166.3, 163.4, 136.2, 133.2, 131.9, 131.8, 130.2, 127.8, 127.3, 126.6, 122.9, 122.7, 113.6, 65.4, 55.4, 27.8, 23.1 ppm; CIMS 312 $[M + NH_4]^+$, 295 $[M + H]^+$; HRMS calcd for $[C_{19}H_{18}O_3 + NH_4]^+$ 312.1600, found 312.1608.

9-Benzylidenefluorene (7). To a −78 °C suspension of benzyltriphenylphosphonium bromide (1.3 g, 3.0 mmol) in 20 mL of THF was added *n*-BuLi (1.1 mL, 2.7 M in hexane, 3.0 mmol), and the mixture was stirred for 1 h at −78 °C. The mixture was warmed to 23 °C and stirred for 1 h. A solution of 9-fluorenone (0.50 g, 2.8 mmol) in 10 mL of THF was added, and the solution was stirred for 6 h at 23 °C and for 1 h at reflux. The mixture was cooled to 23 °C and filtered through a small plug of silica gel eluting with 20:1 hexane−ethyl acetate. The filtrate was concentrated *in vacuo*, and the residue was purified by radial chromatography (4 mm silica plate, hexane) to afford 0.67 g (95%) of **7** as a colorless solid: mp 69 °C; R_f = 0.65 (1:4 ethyl acetate−hexane); ^{1}H NMR ($CDCl_3$, 400 MHz) δ 7.80 (d, 1H, J = 7.3 Hz), 7.73 (m, 3H), 7.58 (m, 3H), 7.47 (t, 2H, J = 7.1 Hz), 7.40 (m, 4H), 7.09 (t, 1H, J = 6.8 Hz) ppm; ^{13}C NMR ($CDCl_3$, 100 MHz) δ 141.2, 139.4, 139.1, 136.8, 136.5, 136.4, 129.2, 128.5, 128.2, 128.0, 127.3, 127.0, 126.6, 124.4, 120.2, 119.7, 119.6 ppm; EIMS 254 $[M]^+$; HRMS calcd for $[C_{20}H_{14}]^+$ 254.1096, found 254.1087.

General Procedure for the Asymmetric Dihydroxylation. A solution of K_2CO_3 (3.00 equiv), $K_3Fe(CN)_6$ (3.00 equiv), $K_2OsO_4 \cdot 2H_2O$ (0.01 equiv), $(DHQD)_2PYDZ$ (**1**) (0.01 equiv), and $CH_3SO_2NH_2$ (only for 1,2-disubstituted and trisubstituted olefins, 1.00 equiv) in *tert*-butyl alcohol−water (1:1) was cooled to 0 °C. The resulting suspension was treated with the corresponding olefin (0.1 M with respect to total reaction volume). The mixture was stirred for the indicated time and quenched by addition of Na_2SO_3. The mixture was stirred for 5 min, warmed to 23 °C over 5 min, and partitioned between ethyl acetate and minimal water. The aqueous layer was extracted three times with ethyl acetate, and the combined organic extracts were washed twice with brine, dried with Na_2SO_4, and concentrated *in vacuo*. Purification of the residue was accomplished by filtration through a silica gel plug, eluting with ethyl acetate or by radial chromatography (4 mm silica gel plate, eluting with hexane−ethyl acetate). Concentration of the appropriate fractions *in vacuo* afforded the indicated yield of product.

Asymmetric Dihydroxylation of α-Methylenetetralin (5). Asymmetric dihydroxylation according to the general procedure using **1** (1 mol %) and $K_2OsO_4 \cdot 2H_2O$ (0.1 mol %) on 0.14 g (0.96 mmol) of **5** at 0 °C for 12 h afforded 0.15 g (90%) of the diol as a colorless solid of 94% ee: mp 133 °C; R_f = 0.33 (1:1 ethyl acetate−hexane); [α] −39 (*c* 0.40, EtOH); ^{1}H NMR ($CDCl_3$, 400 MHz) δ 7.53 (m, 1H), 7.18 (m, 2H), 7.09 (m, 1H), 3.70 (d, 1H, J = 11.4 Hz), 3.65 (d, 1H, J = 11.4 Hz), 2.82 (m, 2H), 2.27 (m, 3H), 1.77 (m, 3H) ppm; ^{13}C NMR ($CDCl_3$, 100 MHz) δ 139.2, 137.7, 128.9, 127.7, 126.6, 126.3, 73.0, 69.2, 33.3, 29.6, 20.2 ppm; CIMS 196 $[M + NH_4]^+$, 178 $[M]^+$, 161, 147; HRMS calcd for $[C_{11}H_{14}O_2 + NH_4]^+$ 196.1338, found 196.1334. The enantiomeric excess was determined by HPLC analysis (Chiralpak AD column, 10% 2-propanol−hexane, 1 mL/min, λ = 254 nm, retention times 11.8 min (minor), 14.1 min (major)).

Asymmetric Dihydroxylation of 1-[[(4-Methoxybenzoyl)oxy]-methyl]-3,4-dihydronaphthalene (6). Asymmetric dihydroxylation according to the general procedure using **1** (1 mol %) and $K_2OsO_4 \cdot 2H_2O$ (1 mol %) on 0.113 g (0.384 mmol) of **6** at 0 °C for 2.75 h afforded 0.040 g (32%) of the diol as a colorless solid of 98% ee and 0.061 (54%) of **6**: R_f = 0.36 (3:1 methylene chloride−ethyl acetate); [α] −20.7 (*c* 1.18, $CHCl_3$); ^{1}H NMR ($CDCl_3$, 400 MHz) δ 7.93 (m, 2H), 7.66 (m, 1H), 7.25 (m, 2H), 7.13 (m, 1H), 6.89 (m, 2H), 4.59 (d, 1H, J = 12.0 Hz), 446 (d, 1H, J = 12.0 Hz), 4.19 (dd, 1H, J = 6.1, 3.5 Hz), 3.85 (s, 3H), 3.36 (bs, 1H), 3.05 (m, 1H), 2.78 (dt, 1H, J = 17.1, 5.8 Hz), 2.78 (bs, 1H), 2.11 (m, 2H) ppm; ^{13}C NMR ($CDCl_3$, 100 MHz) δ 166.5, 163.7, 136.6, 136.2, 131.8, 128.7, 128.1, 127.7, 126.6, 121.9, 113.8, 73.5, 69.0, 68.4, 55.5, 26.1, 25.2 ppm; CIMS 346 $[M + NH_4]^+$, 329 $[M + H]^+$, 311 $[M - OH]^+$, 231, 180, 138; HRMS calcd for $[C_{19}H_{20}O_5 + H]^+$ 329.1389, found 329.1376. The enantiomeric excess was determined by HPLC analysis (Chiralcel OJ column, 15% 2-propanol−hexane, 1 mL/min, λ = 254 nm, retention times 26.7 min (minor), 44.8 min (major)).

Asymmetric Dihydroxylation of 9-Benzylidenefluorene (7). Asymmetric dihydroxylation according to the general procedure using **1** (1

(19) In addition to these lines of evidence which argue against the [2 + 2] pathway, recent studies on the $^{12}C/^{13}C$ kinetic isotope effects at the olefinic linkage in the dihydroxylation reaction provide a compelling case in favor of the CCN model. Corey, E. J.; Noe, M. C., Grogan, M. J. *Tetrahedron Lett*. **1996**, *37*, 4899.

(20) Campbell, M. M.; Abbas, N.; Sainsbury, M. *Tetrahedron* **1985**, *41*, 5637.

mol %), $K_2OsO_4 \cdot 2H_2O$ (0.5 mol %), and $CH_3SO_2NH_2$ (1 equiv) on **7** (0.24 g, 0.96 mmol) gave 0.17 g (61%) of the corresponding diol as a colorless solid of 97% ee and 0.058 g (23%) of recovered **7**: R_f = 0.36 (1:3 ethyl acetate−hexane); mp 126 °C; [α] +8.4 (*c* 0.62, EtOH); ^{1}H NMR ($CDCl_3$, 400 MHz) δ 7.63 (d, 1H, *J* = 7.8 Hz), 7.56 (dd, 1H, *J* = 2.2, 5.1 Hz), 7.35 (m, 2H), 7.27 (m, 4H), 6.96 (t, 1H, *J* = 6.7 Hz), 6.89 (t, 2H, *J* = 7.8 Hz), 6.73 (d, 2H, *J* = 7.2 Hz), 5.26 (s, 1H), 4.89 (b, 2H) ppm; ^{13}C NMR ($CDCl_3$, 100 MHz) δ 145.9, 144.8, 140.2, 140.1, 137.6, 129.3, 129.1, 127.5, 127.3, 127.0, 126.8, 125.7, 124.3, 119.8, 119.6, 84.8, 79.5 ppm; CIMS 306 $[M + NH_4]^+$, 288 $[M]^+$; HRMS calcd for $[C_{20}H_{16}O_2 + NH_4]^+$ 306.1494, found 306.1480. The enantioselectivity was determined by chiral HPLC analysis (Chiralpak AD column, 15% 2-propanol-hexane, 1 mL/min, λ = 254 nm, 23 °C, retention times 16.3 min (*S*), 18.4 min (*R*)).

Asymmetric Dihydroxylation of Phenyldihydronaphthalene (9). Asymmetric dihydroxylation according to the general procedure using **1** (1 mol %), $K_2OsO_4 \cdot 2H_2O$ (0.5 mol %), and methanesulfonamide (1 equiv) on 0.20 g (0.96 mmol) of **9** at 0 °C for 72 h afforded 0.18 g (79%) of the diol (shown in Table 2) as a colorless solid of 77% ee and 0.037 g (19%) of recovered **9**: R_f = 0.59 (1:1 ethyl acetate−hexane); [α] −60.7 (*c* 0.42, EtOH); ^{1}H NMR ($CDCl_3$, 400 MHz) δ 7.29−7.08 (m, 8H), 7.02 (d, 1H, *J* = 7.7 Hz), 4.03 (d, 1H, *J* = 6.6 Hz), 3.15 (s, 1H), 2.98 (dt, 1H, *J* = 5.8, 17.1 Hz), 2.88 (dt, 1H, *J* = 6.9, 18.1 Hz), 2.32 (bs, 1H), 2.03 (m, 1H), 1.90 (m, 1H) ppm; ^{13}C NMR ($CDCl_3$, 100 MHz) δ 145.9, 140.1, 136.4, 130.0, 128.3, 127.9, 127.7, 127.2, 127.1, 126.7, 77.4, 75.4, 26.7, 26.0 ppm; CIMS 258 $[M + NH_4]^+$, 240 $[M]^+$; HRMS calcd for $[C_{16}H_{16}O_2]^+$ 240.1150, found 240.1143. The enantiomeric excess was determined by HPLC analysis (Chiralcel OD column, 15% 2-propanol−hexane, 1 mL/min, λ = 254 nm, 23 °C; retention times 11.8 min (major), 9.2 min (minor)).

Asymmetric Dihydroxylation of 8. Asymmetric dihydroxylation according to the general procedure using **1** (1 mol %), $K_2OsO_4 \cdot 2H_2O$ (0.5 mol %), and methanesulfonamide (1 equiv) on 0.20 g (0.96 mmol) of **8**[21] at 0 °C for 48 h gave 0.21 g (91%) of the corresponding diol (structure shown in Table 2) as a colorless solid of 95% ee: mp 130 °C; R_f = 0.42 (1:1 ethyl acetate−hexane); [α] +62 (*c* 0.33, EtOH); ^{1}H NMR ($CDCl_3$, 400 MHz) δ 7.78 (d, 1H, *J* = 7.5 Hz), 7.61 (d, 1H, *J* = 7.5 Hz), 7.39 (m, 2H), 7.36 (m, 2H), 7.03 (d, 1H, *J* = 7.6 Hz), 3.80 (m, 1H), 3.22 (ddd, 1H, *J* = 2.8, 6.4, 14.6 Hz), 2.77 (m, 1H), 2.42 (d, 1H, *J* = 9.4 Hz), 2.33 (m, 2H), 2.22 (m, 1H) ppm; ^{13}C NMR ($CDCl_3$, 100 MHz) δ 147.7, 142.7, 140.2, 139.6, 135.6, 130.3, 129.2, 128.0, 126.7, 125.4, 120.6, 117.5, 77.7, 72.0, 27.9, 25.8 ppm; EIMS 238 $[M]^+$; HRMS calcd for $[C_{16}H_{14}O_2]^+$ 238.0994, found 238.1003. The enantiomeric excess was determined by HPLC analysis (Chiralpak AD column, 15% 2-propanol−hexane, 1 mL/min, λ = 254 nm, 23 °C; retention times 15.7 min (*R*), 21.8 min (*S*)).

Asymmetric Dihydroxylation of 9-Vinylanthracene (10). Asymmetric dihydroxylation was conducted according to the general procedure using **1** (1 mol %) and $K_2OsO_4 \cdot 2H_2O$ (0.01 mol %) on 0.80 g (3.92 mmol) of **10** at 0−4 °C. After this mixture was stirred for 4 days, 3 g of Na_2SO_3 was added, and the mixture was diluted with 50 mL of water. The aqueous mixture was extracted three times with 50 mL of CH_2Cl_2. The combined organic layers were dried over anhydrous Na_2SO_4, filtered, and concentrated *in vacuo*. The residue was filtered through a pad of silica gel, eluting with 1:1 ethyl acetate−hexane, to afford 0.70 g (75%) of the corresponding diol (structure shown in Table 2) as a yellow solid: mp 133.5 °C; [α] −6.4 (*c* 0.22, EtOH); R_f = 0.34 (50% ethyl acetate−hexane); ^{1}H NMR ($CDCl_3$, 500 MHz) δ 8.66 (d, 2H, *J* = 8.7 Hz), 8.44 (s, 1H), 8.01 (d, 2H, *J* = 8.0 Hz), 7.51 (m, 2H), 7.46 (m, 2H), 6.40 (dt, 1H, *J* = 9.7, 3.0 Hz), 4.48 (dt, 1H, *J* = 3.4, 11.8 Hz), 3.94 (m, 1H), 2.75 (d, 1H, *J* = 2.3 Hz), 2.35 (dd, 1H, *J* = 3.8, 8.0 Hz) ppm; ^{13}C NMR ($CDCl_3$, 100 MHz) δ 131.6, 130.3, 129.9, 129.3, 128.7, 125.9, 124.8, 124.6, 72.5, 66.1 ppm; FABMS 261 $[M + Na]^+$; HRMS calcd for $[C_{16}H_{14}O_2 + H]^+$ 261.0892, found 261.0890. The enantioselectivity was determined by HPLC analysis (Chiralcel OD column, 10% 2-propanol−hexane, λ = 254 nm; retention times 26.7 min (*R*), 40.2 min (*S*)). To a solution of the above diol (0.010 g, 0.042 mmol) in 0.2 mL of CH_2Cl_2 was added pyridine (0.0079 g, 0.10 mmol) and acetic anhydride (0.010 g, 0.10 mmol), and the resulting solution was stirred at 23 °C for 24 h. The mixture was taken up in 2 mL of 1 M HCl, and the aqueous layer was extracted with 10 mL of ether. The organic layer was washed with 2 mL of saturated $NaHCO_3$, dried over anhydrous $MgSO_4$, filtered, and concentrated *in vacuo*, giving 0.012 g (90%) of the diacetate as a yellow solid. mp 86.5−87.5 °C; [α] −38.6 (*c* 1.00, EtOH); R_f = 0.52 (50% ether−hexane); ^{1}H NMR ($CDCl_3$, 500 MHz) δ 8.60 (b, 2H), 8.47 (s, 1H), 8.01 (d, 2H, *J* = 8.0 Hz), 7.59 (m, 2H), 7.55 (m, 1H), 7.46 (m, 2H), 5.04 (dd, 1H, *J* = 9.6, 12.2 Hz), 4.51 (dd, 1H, *J* = 3.8, 12.2 Hz), 2.12 (s, 3H), 2.10 (s, 3H) ppm; ^{13}C NMR ($CDCl_3$, 100 MHz) δ 170.8, 170.2, 131.5, 130.0, 129.5, 129.3, 126.7, 126.5, 124.9, 77.3, 70.4, 65.3, 21.0, 20.8 ppm; EIMS 322 $[M]^+$, 207; HRMS calcd for $[C_{20}H_{18}O_4]^+$ 322.1205, found 322.1204.

To a mixture of the above diacetate (0.012 g, 0.037 mmol), *N*-bromosuccinimide (0.007 g, 0.04 mmol), and 0.1 mL of CCl_4 was added a crystal of iodine, and the mixture was stirred for 3 h at 75 °C. The mixture was cooled to 23 °C, and the resulting 10-bromo derivative diacetate was isolated by preparative TLC (1:1 ethyl acetate−hexane). The material thus obtained was taken up in 5 mL of methanol, and 0.1 g of KOH was added. Cleavage of the acetate groups was complete within 5 min. The mixture was concentrated *in vacuo* and partitioned between 1 mL of water and 2 mL of CH_2Cl_2. Further extraction of the aqueous layer with CH_2Cl_2 (2 × 2 mL) gave 0.010 g (84%) of 1-(10-bromo-9-anthracenyl)ethane-1,2 diol as a colorless solid: mp 112.5 °C dec; [α] −2.9 (*c* 0.35, EtOH); R_f = 0.34 (50% ethyl acetate−hexane); ^{1}H NMR ($CDCl_3$, 500 MHz) δ 8.68 (d, 2H, *J* = 7.8 Hz), 8.61 (d, 2H, *J* = 8.0 Hz), 7.58 (m, 2H), 7.50 (m, 2H), 6.47 (m, 1H), 4.48 (dd, 1H, *J* = 9.6, 12.2 Hz), 3.93 (dd, 1H, *J* = 3.8, 12.2 Hz), 2.94 (s, 1H), 2.48 (s, 1H) ppm; FABMS 339 $[M + Na]^+$, 316 $[M + H]^+$.

Acknowledgment. This research was supported by an NSF Fellowship to M.C.N. and an NSF grant to E.J.C. We are grateful to Mr. Angel Guzman-Perez for preparing and testing compound **6**.

JA961233M

(21) (a) Rastetter, W. H.; Nachbar, R. B.; Russo-Rodriguez, S.; Wattley, R. V.; Thilly, W. G.; Andon, B. M.; Jorgensen, W. L.; Ibrahim, M. *J. Org. Chem.* **1982**, *47*, 4873. (b) Steinberg, E.; Conrad, G. A.; Ruddy, A. W. *J. Am. Chem. Soc.* **1954**, *76*, 5445.